

# From Pixels to Nanometers: Integrating Machine Learning and Mechatronics for Photolithography Automation with a Focus on 2D Materials

A Thesis

submitted to

Indian Institute of Science Education and Research Pune

in partial fulfillment of the requirements for the

BS-MS Dual Degree Programme

by

Ravi Prakash Rao



Indian Institute of Science Education and Research Pune

Dr. Homi Bhabha Road,

Pashan, Pune 411008, INDIA.

December, 2023

Supervisor: Dr. Atikur Rahman

© Ravi Prakash Rao 2023

All rights reserved

# Certificate

This is to certify that this dissertation entitled From Pixels to Nanometers: Integrating Machine Learning and Mechatronics for Photolithography Automation with a Focus on 2D Materials towards the partial fulfilment of the BS-MS dual degree programme at the Indian Institute of Science Education and Research, Pune represents study/work carried out by Ravi Prakash Rao at Indian Institute of Science Education and Research under the supervision of Dr. Atikur Rahman, Deputy Chair / Associate Professor, Department of Physics, during the academic year 2022-2023.



Dr. Atikur Rahman

Committee:

Dr. Atikur Rahman

Dr. Shouvik Datta

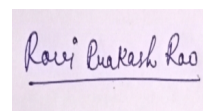


*This thesis is dedicated to my friends, family, labmates, my supervisor, and to my late father.*



# Declaration

I hereby declare that the matter embodied in the report entitled From Pixels to Nanometers: Integrating Machine Learning and Mechatronics for Photolithography Automation with a Focus on 2D Materials are the results of the work carried out by me at the Department of Physics, Indian Institute of Science Education and Research, Pune, under the supervision of Dr. Atikur Rahman and the same has not been submitted elsewhere for any other degree.

A rectangular box containing a handwritten signature in black ink. The signature reads "Ravi Prakash Rao" and is underlined.

Ravi Prakash Rao





# Acknowledgments

I would like to extend my heartfelt gratitude to all those who have supported and guided me throughout my MS project journey. Special thanks go to my supervisor, Dr. Atikur Rahman, whose unwavering support has been a constant since I joined the Nano-Q lab in January 2021. His boundless passion for physics has been a prominent source of inspiration. Whenever I needed motivation, faced challenges with my ideas, or encountered theoretical and experimental hurdles, Prof. Atikur was there to provide guidance. The student-mentor relationship I share with Prof. Atikur has been genuinely exceptional, allowing me to explore various aspects of instrumentation and experimental condensed matter physics.

I also want to express my deep appreciation to my thesis supervisor, Dr. Shouvik Datta, for their invaluable expertise and input.

Furthermore, I'm grateful for the valuable insights and contributions of Dr. Vrinda Narayanan, Gokul MA, Suraj Lakhchaura, and all my other lab mates. The engineering team at H-cross, notably Technical Officer Nilesh Dumbre and Technical Assistant Karthikeyan S, provided invaluable assistance.

I extend my thanks to Prof. G.V. Pavan Kumar and his student Ashutosh Shukla for their contributions to the Raman Spectra measurements.

Last but certainly not least, I consider myself fortunate to have such an amazing group of friends, including my labmates and my family, whose unwavering support made completing

this thesis possible.

# Abstract

We have tried to optimize the growth parameters of the CVD growth of  $\text{Bi}_2\text{O}_2\text{Se}$  on various substrates, focusing on f-mica. Also, exploring the various techniques of Photolithography to signify the vital role it plays in 2D material research. Moreover, we have proposed and designed an Automated Maskless Photolithography setup by modifying the existing Photolithography setup with merely Stepper Motors, Raspberry Pi, Arduino, A camera and a DLP.



# Contents

<b>Abstract</b>	<b>xi</b>
0.1 A guide to read this thesis. . . . .	4
<b>1 Introduction</b>	<b>5</b>
1.1 Background Information: Introduction to Two Dimensional(2D) materials . . . . .	5
1.2 From Dust to Devices . . . . .	7
<b>2 Photolithography under a Physicist’s Microscope</b>	<b>11</b>
2.1 Photolithography as an essential tool . . . . .	11
2.2 UV Lithography . . . . .	14
2.3 E-Beam Lithography . . . . .	16
<b>3 More about 2D materials, and motivation for AMPS</b>	<b>19</b>
3.1 Bismuth Oxyselenide . . . . .	19
3.2 The Initial ”positive” Results of an Unsuccessful Project . . . . .	24
<b>4 Automated Maskless Photolithography Setup(AMPS)</b>	<b>27</b>
4.1 The Existing Photolithography Setup . . . . .	27
4.2 The Proposed Modifications . . . . .	28

4.3	Workflow of AMPS (Automated Maskless Photolithography System) . . . . .	30
4.4	Instrumentation . . . . .	31
<b>5</b>	<b>Conclusion and Future Prospects</b>	<b>43</b>
5.1	Two-Dimensional Bi <sub>2</sub> O <sub>2</sub> Se/MoS <sub>2</sub> Heterostructures . . . . .	43

# List of Figures

1.1	Schematic of CVD tube for the growth of Bismuth Oxyselenide . . . . .	7
1.2	The working of Photolithography . . . . .	8
2.1	The current technological state of art of photolithography [1] . . . . .	12
2.2	a) Schematic of a UV-LED photolithography system [2]. . . . .	13
2.3	a)Tessar projection photolithography. b) Microscope projection photolithography setup [3] . . . . .	14
2.4	A typical EBL setup, comprising a chamber, an electron source, and a column that houses all the electron optics essential for electron beam focusing, scanning, and beam control, including its activation and deactivation.[4] . . . . .	17
3.1	Schematic of CVD growth of $\text{Bi}_2\text{O}_2\text{Se}$ . . . . .	19
3.2	CVD growth of $\text{Bi}_2\text{O}_2\text{Se}$ layers on f-mica a) Very few layers but smaller size(mag.=100x) b) Thick plate and larger size(mag.=10x) c) Thinner plate and larger size(mag.=50x) d)Thinner plate and larger size(mag.=50x) . . . . .	20
3.3	The Observed Raman Spectra of the grown $\text{Bi}_2\text{O}_2\text{Se}$ . . . . .	21
3.4	The Observed Raman peak at $157.5 \text{ cm}^{-1}$ resulting from $A_{1g}$ vibrational mode of the grown $\text{Bi}_2\text{O}_2\text{Se}$ . . . . .	21
3.5	The Observed Raman peak at $157.5 \text{ cm}^{-1}$ resulting from $A_{1g}$ vibrational mode of the grown $\text{Bi}_2\text{O}_2\text{Se}$ . . . . .	22
3.6	The Observed Raman Spectra of the grown $\text{Bi}_2\text{O}_2\text{Se}$ . . . . .	22

3.7	a) AFM images of crystals of $\text{Bi}_2\text{O}_2\text{Se}$ grown on mica and the following thickness profile of the same(few layers)	23
3.8	a) AFM images of crystals of $\text{Bi}_2\text{O}_2\text{Se}$ grown on mica and the following thickness profile of the same(nanoplates)	23
3.9	a) AFM images of crystals of $\text{Bi}_2\text{O}_2\text{Se}$ grown on mica and the following thickness profile of the same(thick plates)	24
3.10	The Raman Spectra of thick plates grown on Si	25
3.11	The Raman Spectra of thin plates grown on mica in the same trial as above	25
3.12	Optical Images of the CVD Growth of $\text{Bi}_2\text{O}_2\text{Se}$ crystals on a) Gold coated Si substrate at 100x, b) Only on Si substrate 100x	26
3.13	FSEM images of the CVD Growth of thin crystals of $\text{Bi}_2\text{O}_2\text{Se}$ on Si substrate	26
3.14	a) AFM images of crystals of $\text{Bi}_2\text{O}_2\text{Se}$ grown on Si b)The thickness profile of a $\text{Bi}_2\text{O}_2\text{Se}$ crystal	26
4.1	Schematic of the current photolithography setup	28
4.2	The Schematic of the Automated Maskless Photolithography Setup	29
4.3	a) Image Acquisition	32
4.4	b) Object Detection	32
4.5	c) Programmed Photolithography	33
4.6	c) The initial results of the DLP Photolithography	33
4.7	The motorized stage	34
4.8	The schematic model of NEMA 17 motor	35
4.9	The schematic A4988 driver	35
4.10	The circuit diagram for Stepper Motors	37
4.11	The schematic of Digital Light Processing	38
4.12	The two DMD pixels [5]	39



4.13 Aluminium Timing Pulleys a) 6mm Belt Width 60 teeth b)6mm Belt Width  
20 Teeth ..... 40

## 0.1 A guide to read this thesis.

The thesis follows this organizational structure:

- **Chapter 1:** This is an introduction section, where we have introduced 2D Materials, CVD, which is one of the leading ways of synthesizing 2D materials, and then Photolithography.
- **Chapter 2:** In this section, we explore the role of photolithography in device making and, thus, the research in 2D materials. We also discuss UV and E-Beam Lithography techniques to understand the photolithography process in detail.
- **Chapter 3:** In this chapter, we divert our focus to an interesting 2D material, Bismuth Oxyselenide. We discuss the whole process from material synthesis to device making thus, we also find our motivation to modify the existing photolithography setup
- **Chapter 4:** In this chapter, we discuss our proposed setup, Automated Maskless Photolithography Setup (AMPS). We focus on the workflow and instrumentation in detail.
- **Chapter 5:** In this chapter, we present some concluding remarks and some immediate and some future prospects to move towards.

# Chapter 1

## Introduction

### 1.1 Background Information: Introduction to Two Dimensional(2D) materials

Two-dimensional (2D) materials are crystalline solids characterized by their unique geometry, with lateral dimensions ranging from 1–10,000  $\mu\text{m}$  and an ultra-thin thickness of less than 1 nm [6]. For five decades, researchers worked extensively to isolate monolayer graphene; it was finally achieved in 2004 when Andre Geim’s team at Manchester University successfully exfoliated it. Graphene still stands as the most renowned 2D material, distinguished by its semimetal nature with a zero bandgap, which allows electrons to move freely, resulting in remarkable conductivity.[7].

Since then, 2D materials have gained remarkable prominence due to their exceptional properties, potential applications in optoelectronics, and the transformative shifts in their physical and chemical characteristics arising from the quantum size effect due to their nanoscale thickness. The confinement of transport carriers and photons to a 2D plane leads to the emergence of extraordinary electrical and optical properties [8].

The realm of 2D materials encompasses a wide array of compositions, including elements from the periodic table. Among them, transition metal dichalcogenides (TMDCs) hold a significant position. In their bulk forms, TMDCs exhibit fascinating properties like magnetism, charge density waves, and superconductivity, which have captivated the attention of researchers worldwide for decades. TMDCs consist of a monolayer of metal atoms interposed between two layers of chalcogen atoms, forming the fundamental monolayer unit. Among 2D TMDCs, particular focus is placed on the semiconducting subgroup. This subset typically features transition metals such as Mo or W combined with chalcogen atoms like S or Se and has gained considerable interest due to its potential in electronic and optoelectronic applications, owing to their direct band gap and lack of centro-symmetry in its lattice structure[9].

Furthermore,  $\text{Bi}_2\text{O}_2\text{Se}$  has emerged as a promising 2D material. Studies have reported carrier mobility as high as  $\tilde{20,000} \text{ cm}^2\text{V}^{-1}\text{s}^{-1}$  at 1.9 K[10], which is even comparable to CVD grown graphene [11]. It is attributed to the unique crystal structure of  $\text{Bi}_2\text{O}_2\text{Se}$ , which consists of alternating  $\text{Bi}_2\text{O}_2$  and Se layers, resulting in a weak interlayer coupling and reduced scattering of charge carriers. Moreover, the bandgap can be adjusted by varying the thickness of the material or applying strain. Experimental measurements have shown that the bandgap of  $\text{Bi}_2\text{O}_2\text{Se}$  can be tuned from 1.8 eV to 2.09 eV. [12]. The presence of heavy Bi atoms and the large spin-orbit coupling in  $\text{Bi}_2\text{O}_2\text{Se}$  result in strong optical absorption and efficient generation of photoexcited carriers. Experimental studies have demonstrated a high absorption coefficient of approximately  $10^5 \text{ cm}^{-1}$  near infrared.

## 1.2 From Dust to Devices

### 1.2.1 Introduction to CVD

Chemical vapor deposition (CVD) and exfoliation are leading pathways to obtain or deposit thin layers of materials, even to one layer for some materials like TMDCs. CVD still holds a significant position in the research of 2D materials. It can be shown by its pivotal role in the Nobel Prize-winning research on blue light-emitting diodes in 2014, which involved the epitaxial growth of gallium nitride through CVD [13]. There are various types of CVDs depending on the nature of the substrates and the environment of the reaction. The most common ones are Atmospheric Pressure (AP) CVD, Low Pressure (LP) CVD, Metal Organic (MO) CVD, etc. But they have one thing in common: they use higher temperatures to provide the energy necessary for a chemical reaction that results in the formation of a thin film on the substrate.

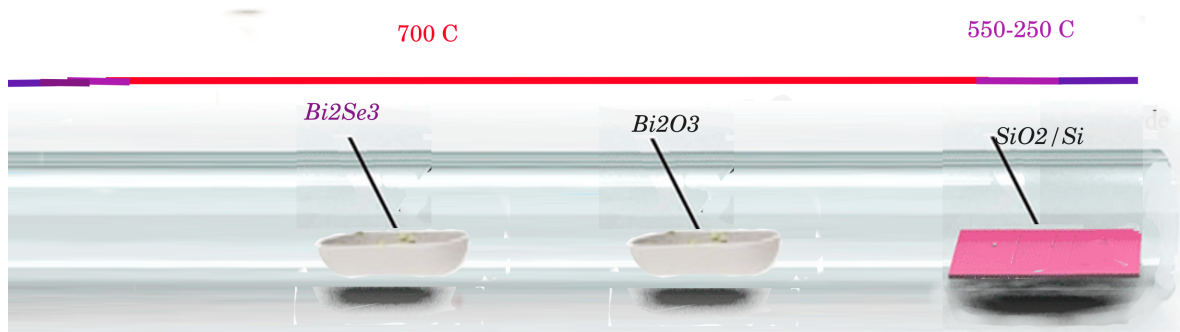


Figure 1.1: Schematic of CVD tube for the growth of Bismuth Oxyselenide

In APCVD setup very similar to **Figure 1.1**, the temperature is raised above the sublimation point of the precursor materials (in the case of Bismuth Oxyselenide, they are Bismuth Selenide and Bismuth oxide powders). Thus, they turn into the gaseous reactants, which are carried by mostly inert gas such as nitrogen into the reaction chamber, but sometimes we use forming gas or oxygen to favor specific reactions. The reacted material is then adsorbed

at the surface, and these adatoms create more adsorption sites depending on the surface interaction, leading to a thin layer or 2D material deposition. The surface interactions play a vital role to the extent that materials favor growth on only particular types of substrates. In our case,  $\text{Bi}_2\text{O}_2\text{Se}$  favors growth on f-mica primarily.

## 1.2.2 Photolithography

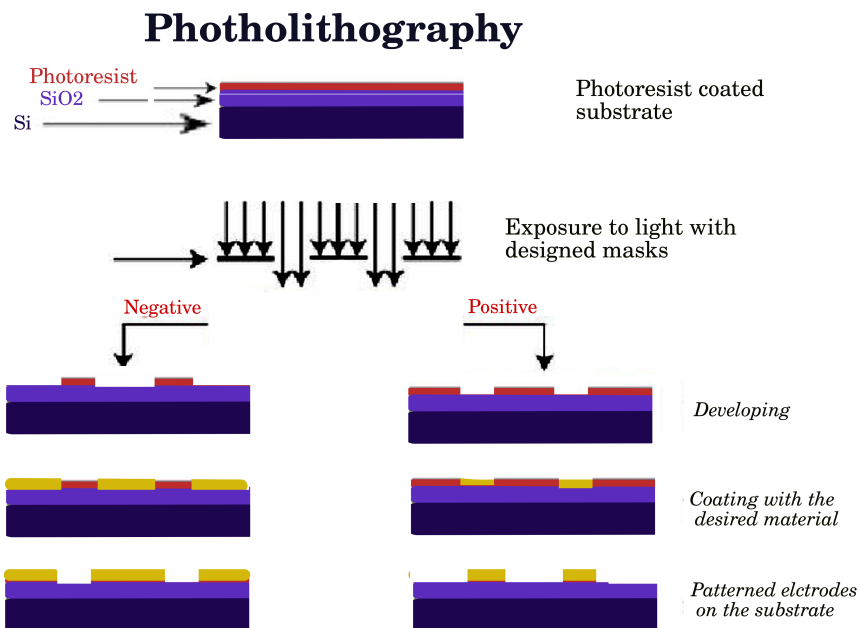


Figure 1.2: The working of Photolithography

Photolithography is a widely used optical technique for imprinting patterns onto a substrate. This fundamental principle applies across various photolithography methods. The process begins with applying a photoresist onto the substrate's surface. Subsequently, the substrate is subjected to electromagnetic radiation, leading to alterations in the molecular structure. This, in turn, influences the material's solubility while a pattern mask is placed over it. Following exposure, etching processes are conducted. The treated substrate is then immersed in a developer solution, typically an aqueous solution. This developer solution acts to dissolve the regions of the photoresist that were exposed to light[14]. To better illustrate

this process, **Figure 1.2** is a schematic representation.

Although, there are other types of photolithographic systems like Electron Beam lithography, Laser Writer, and maskless photolithography setups, which are very expensive ( USD 100,100., USD 100,000 and USD 1,000,000, respectively) and time consuming[15].





# Chapter 2

## Photolithography under a Physicist's Microscope

### 2.1 Photolithography as an essential tool

We have already been introduced to Photolithography in chapter1, and it sounds interesting, as Photolithography can be roughly translated to "printing using light." But for most us experimental physicists, it is merely a tool to get the desired patterned electrodes on our thin layer or chosen 2D material, so we can finally study all sorts of fascinating physics at nanoscales and even at near-zero Kelvin temperatures for the enhanced quantum effect, as the temperature decreases, the effects due to the quantization of energy levels, the increasing significance of wave-particle duality, quantum tunneling, and adherence to Bose-Einstein or Fermi-Dirac statistics becomes more pronounced as the thermal energy can no longer mask the inherent quantum behaviors of particles. We also use these nanodevices to research for immediate and vast practical applications in the semiconductor or energy sector. Now, we will discuss the current technological development in photolithography.

These developments in lithography techniques have pushed the boundaries of resolution.

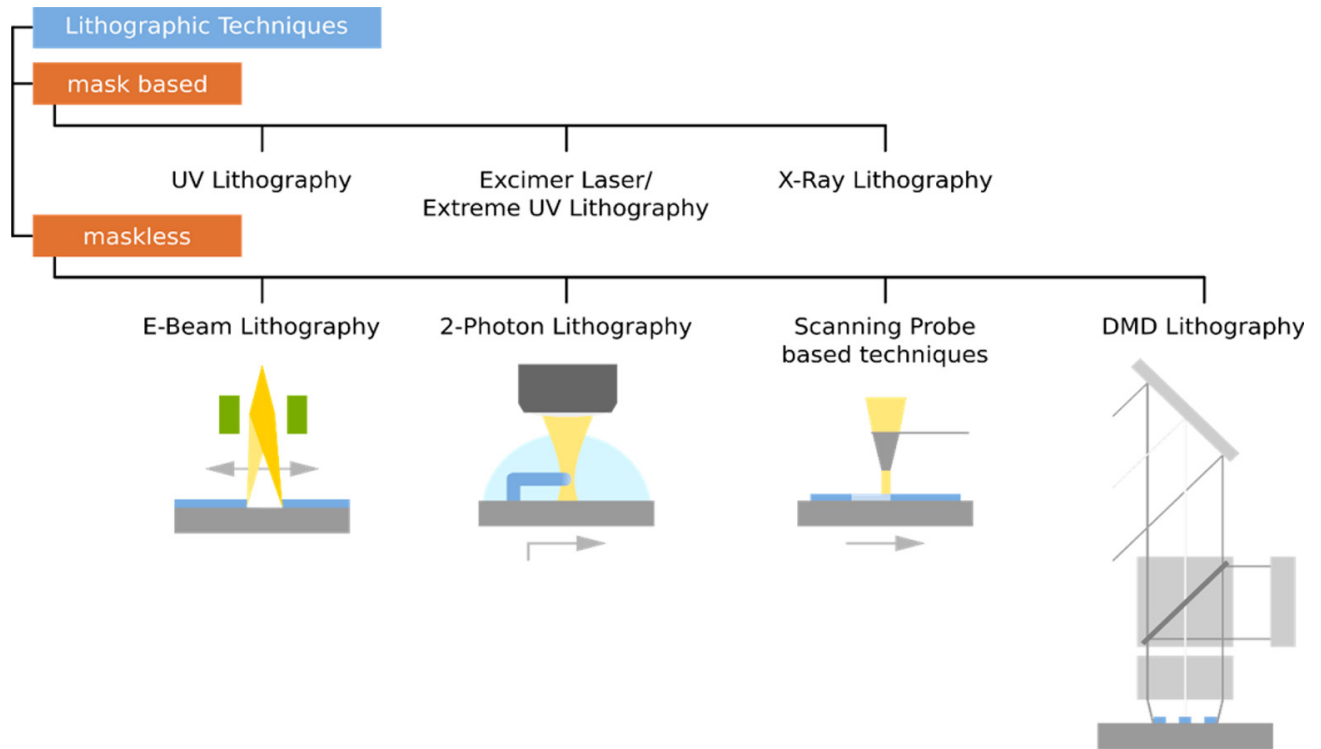


Figure 2.1: The current technological state of art of photolithography [1]

Traditional lithography methods offer resolutions as fine as 7 nanometers. Very recently, cutting-edge approaches like Advanced Semiconductor Material Lithography (AMSL) and innovations proposed by Taiwan Semiconductor Manufacturing Company (TSMC) aim to achieve even finer resolutions, targeting dimensions below 3 nanometers [16].

However, these technological marvels are still an art(i.e., not having access) to most of the condensed matter physics labs owing to their really expensive cost and the fact that they are only present in a handful of labs. We will discuss the working of UV Lithography and E-Beam Lithography to understand the overall working principles of photolithography.

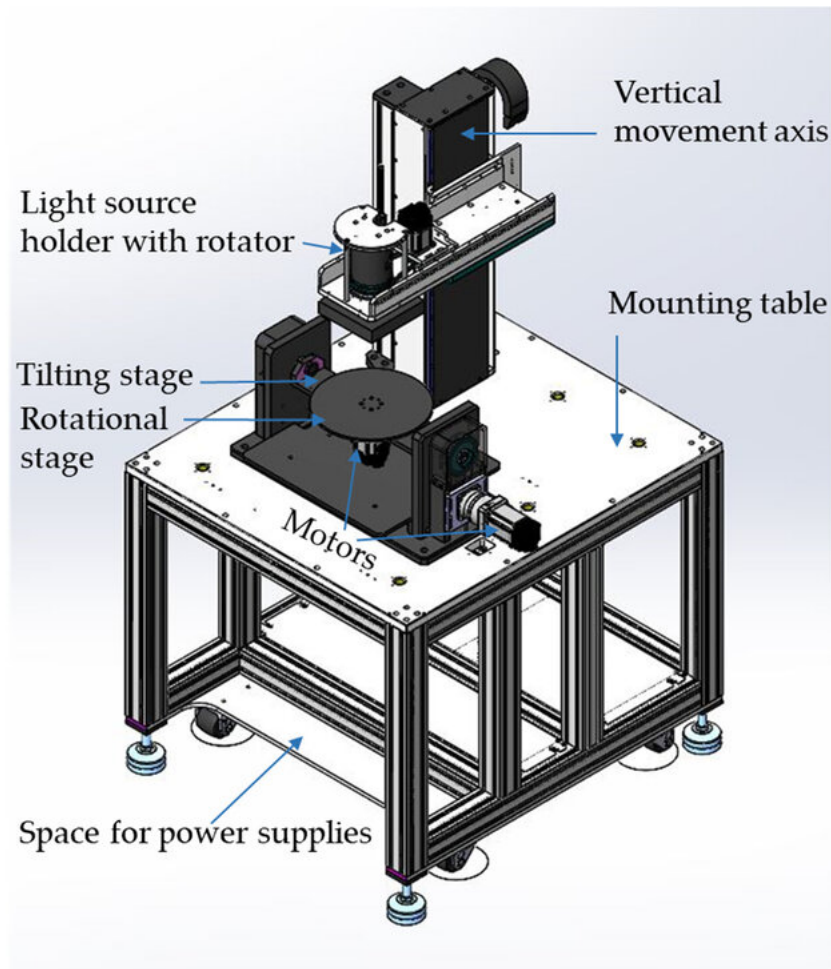


Figure 2.2: a) Schematic of a UV-LED photolithography system [2].

## 2.2 UV Lithography

UV photolithography is a common approach for manufacturing microscale designs on diverse materials, thanks to its ability to create precise geometries and patterns. Typically, this method involves illuminating a silicon wafer coated with a photoresist with near-UV light, typically at wavelengths of 365 or 405 nm, via a mask bearing the desired pattern. This mask selectively permits light to pass through the wafer, reproducing the pattern on the photoresist. **Figure 2.2** shows the instrumentation of one such setup. However, due to the constraints imposed by the wavelength of light used, it's typically not feasible to produce nanoscale structures using this technique [3]. But like every time, the physicists have found ways to break this limit. We will discuss one of the many similar innovative approaches.

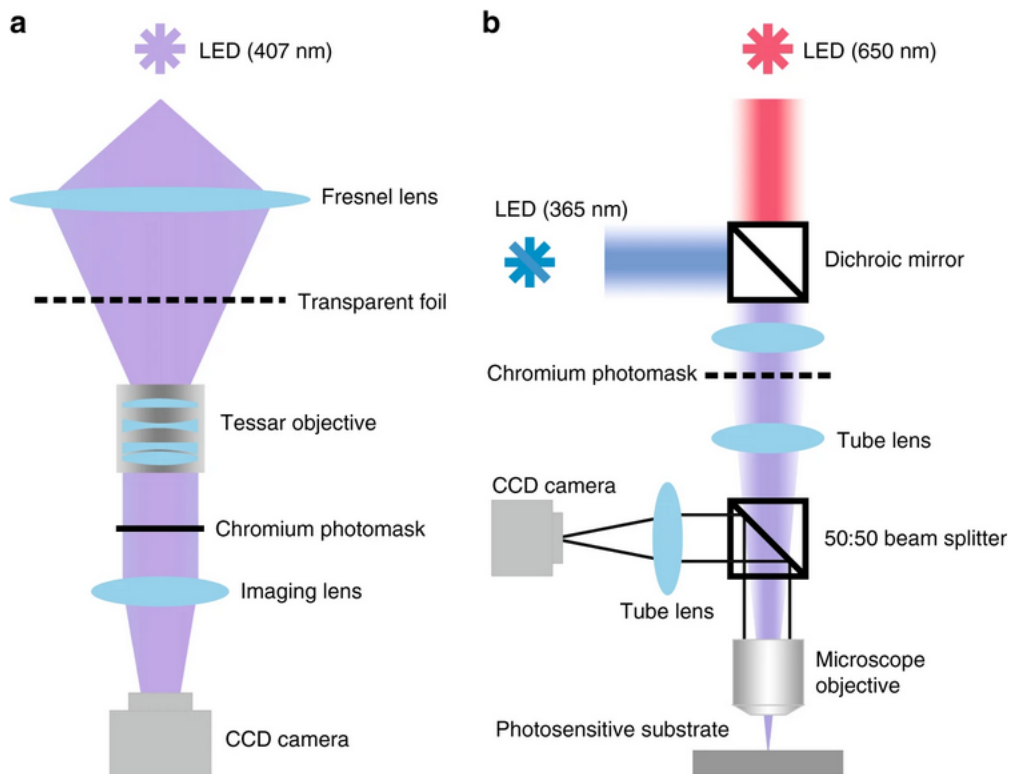


Figure 2.3: a) Tessar projection photolithography. b) Microscope projection photolithography setup [3]

This whole process can be established as a sequence comprising three primary steps,

commencing with structure design. The desired micro- and nanostructures were designed using vector-graphics software, followed by their printing onto a transparent polymer foil containing photosensitive silver layers via a high-resolution laser plotter. The printing offers an effective resolution of 10  $\mu\text{m}$  to the structures.

The second step involves Tessar projection photolithography to transfer the printed patterns onto chromium photomasks. The TPP setup involves a high-power UV-LED placed at the focal plane of a Fresnel lens to expose photopolymer on the chromium mask. A 10x Tessar objective with a 50 mm focal length demagnifies the patterns onto the chromium mask. This mask is prepared with a wet-etch-resistant photopolymer layer. After irradiation and development, the structural pattern is etched into the chromium layer. Finally, the photomask is cleaned, yielding a patterned photomask.

In the last step, microscope projection photolithography (MPP) fabricates micro- and nanostructures. The setup involves a high-power UV-LED for exposure, and the photomask with the desired structure pattern is placed in the image plane of the microscope objective, allowing the structural image on the photomask to be projected onto a tube lens below. Thus, using this brilliant setup, one can fabricate nanodevice structures with feature sizes as small as  $\sim 150\text{nm}$  [2]. But from the whole process, we can see how important of a role photolithography plays in making devices at nanoscales. Moreover, it can be seen how much time and resource-consuming the process is, and excellent precision is needed throughout. Hence, even for most labs that have access to this highly advanced UV-LED lithography system, photolithography seems to be acting like a bottleneck(rate-limiting step) in the process of nanodevice making; thus, the experimental research on 2D materials.

## 2.3 E-Beam Lithography

Electron Beam Lithography (or simply EBL) is a sophisticated nanofabrication technique that relies on a finely focused beam of electrons to pattern a surface coated with an electron-sensitive resist material. The core strength of e-beam lithography lies in its ability to produce features at the nanoscale, with resolutions down to a few nanometers. This extreme precision is primarily achieved due to the wave nature of electrons. E-beam lithography works on the principle of focusing a fine beam of electrons onto a substrate coated with an electron-sensitive resist material. The electrons expose the resist, selectively modifying it. Subsequent development steps result in high-resolution patterns [17].

However, this technique has its resolution limits. These limitations are often associated with the scattering of electrons, proximity effects, and electron beam-induced damage to the substrate and resist material. Overcoming these challenges often necessitates complex strategies like multiple exposures, corrections, and advanced resists.

This process involves several key steps, each contributing to the remarkable precision and resolution of the final patterns.

- **Electron Beam Source:** EBL begins with an electron beam source, typically generated by thermionic emission or field emission from a sharp metal tip. The electron gun generates a stream of electrons, which is then focused into a narrow beam using electromagnetic lenses. This high-energy electron beam is what ultimately exposes the resist material.
- **Electron-Sensitive Resist:** The substrate, often a semiconductor wafer or other solid material, is coated with an electron-sensitive resist. This resist is a polymer material that undergoes chemical changes when exposed to electrons. It hardens or softens depending on the type of resist (positive or negative) and the energy of the incident electrons.

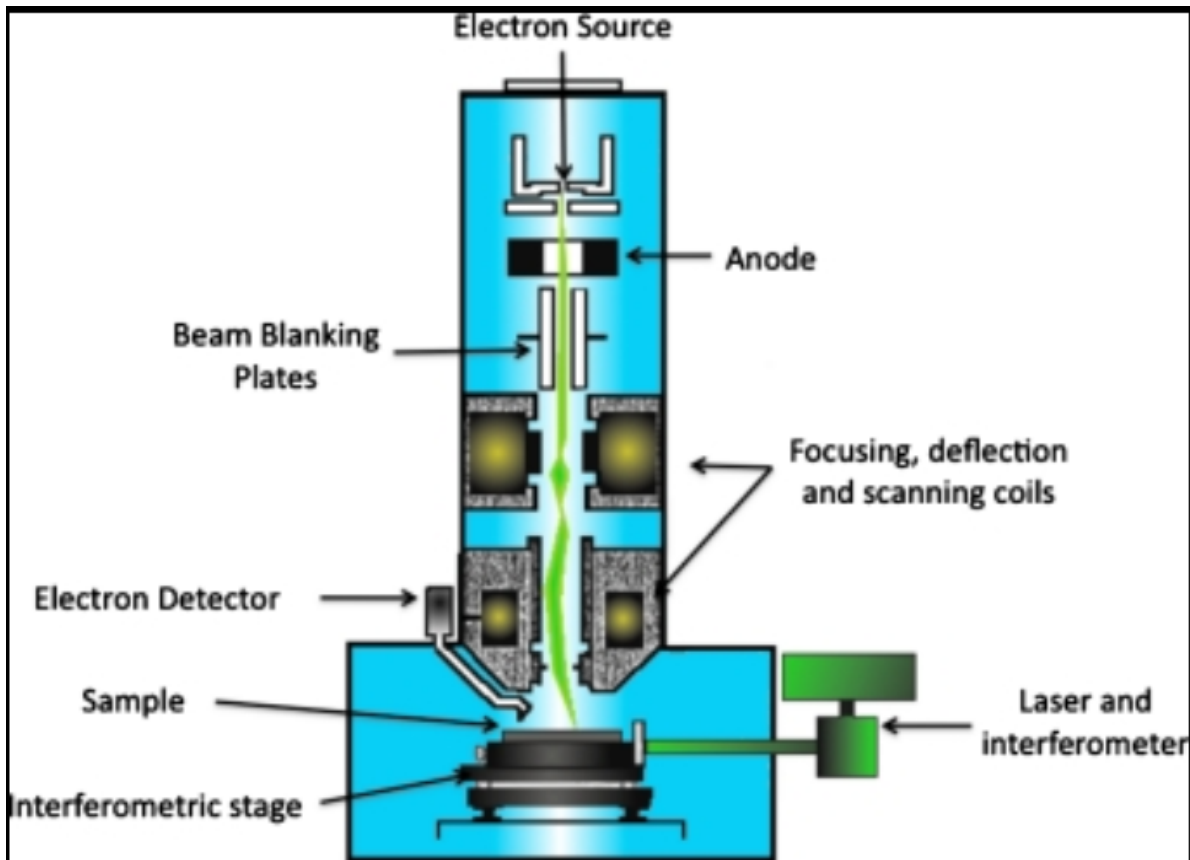


Figure 2.4: A typical EBL setup, comprising a chamber, an electron source, and a column that houses all the electron optics essential for electron beam focusing, scanning, and beam control, including its activation and deactivation.[4]

- **Electron Beam Scanning:** The focused electron beam is scanned across the resist-coated substrate in a precise pattern. This scanning is meticulously controlled by electromagnetic coils, allowing the beam to trace out intricate shapes and structures.
- **Exposure:** When the high-energy electrons hit the resist, they induce chemical reactions in the material. In positive resist, exposure results in cross-linking of the polymer, making it more resistant to subsequent processing steps. In negative resist, exposure softens the polymer, making it easier to remove.
- **Development:** After exposure, the substrate undergoes a development step, where the exposed or unexposed regions of the resist are selectively removed. This leaves behind the desired pattern, faithfully reproducing the electron beam's path.
- **Etching or Deposition:** Depending on the application, the patterned resist can serve as a mask for further processing steps. In semiconductor manufacturing, for instance, the exposed areas may be etched to create features, or materials may be deposited onto the exposed areas.

Electrons exhibit particle-like and wave-like characteristics, and their short wavelengths at high energies allow for incredibly fine resolution. Unlike photolithography, which uses light and is constrained by the diffraction limit, EBL can achieve much smaller feature sizes, as small as 4 nm [18]. However, the scanning is strictly a serial writing process, slowing the e-beam lithography. The limited throughput of e-beam lithography primarily confines its practical uses to generating photomasks or creating distinctive features.



# Chapter 3

## More about 2D materials, and motivation for AMPS

### 3.1 Bismuth Oxyselenide

#### 3.1.1 CVD Growth of $\text{Bi}_2\text{O}_2\text{Se}$

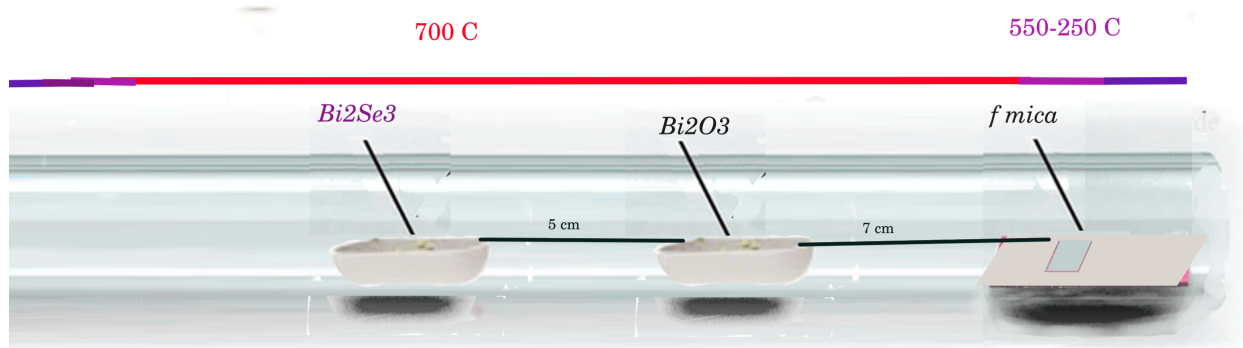


Figure 3.1: Schematic of CVD growth of  $\text{Bi}_2\text{O}_2\text{Se}$

As discussed earlier, we have used mica as a substrate because of its strong VdW strength,

and it forms an attractive interfacial interaction with  $\text{Bi}_2\text{O}_2\text{Se}$ . Hence, it facilitates growth easily.

### 3.1.2 Characterization of the grown thin layers of $\text{Bi}_2\text{O}_2\text{Se}$

First, we present the optical images of the grown samples.

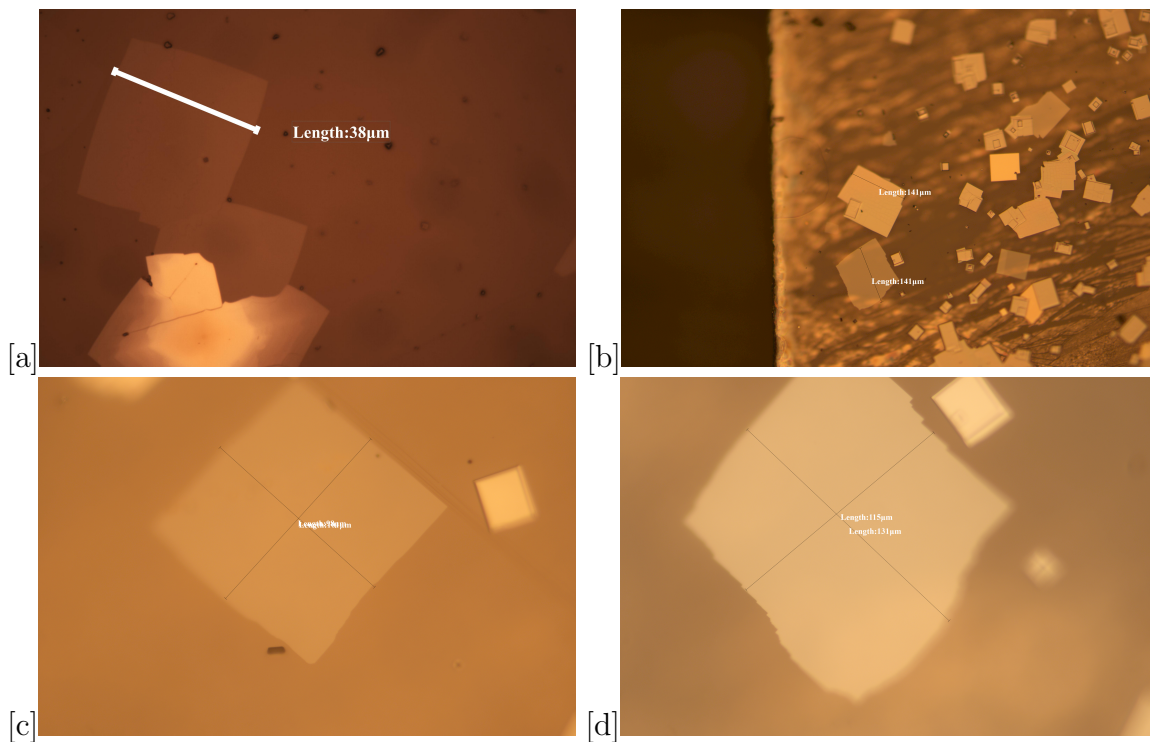


Figure 3.2: CVD growth of  $\text{Bi}_2\text{O}_2\text{Se}$  layers on f-mica a) Very few layers but smaller size(mag.=100x) b) Thick plate and larger size(mag.=10x) c) Thinner plate and larger size(mag.=50x) d)Thinner plate and larger size(mag.=50x)

Now, we present the observed Raman spectra of the grown samples, and we have used spline smoothing in Python to construct an interpolating function of the data from which we can identify the peak.

However, this strong interaction has drawbacks; it is tough to transfer to other substrates to study its optoelectrical properties. Hence, we also tried to grow  $\text{Bi}_2\text{O}_2\text{Se}$  directly on

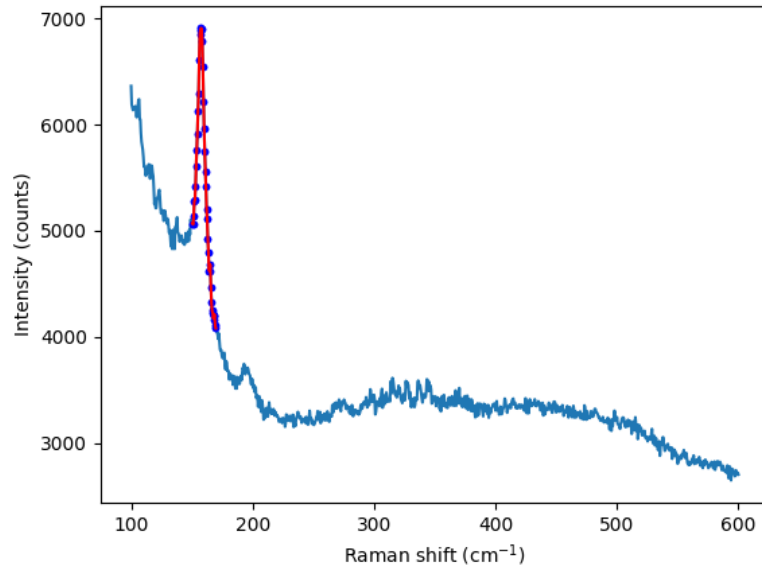


Figure 3.3: The Observed Raman Spectra of the grown  $\text{Bi}_2\text{O}_2\text{Se}$

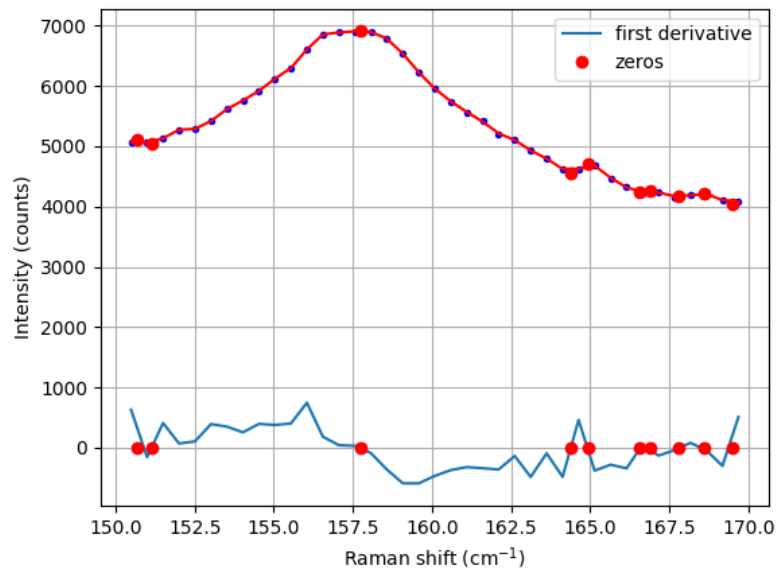


Figure 3.4: The Observed Raman peak at  $157.5 \text{ cm}^{-1}$  resulting from  $A_{1g}$  vibrational mode of the grown  $\text{Bi}_2\text{O}_2\text{Se}$

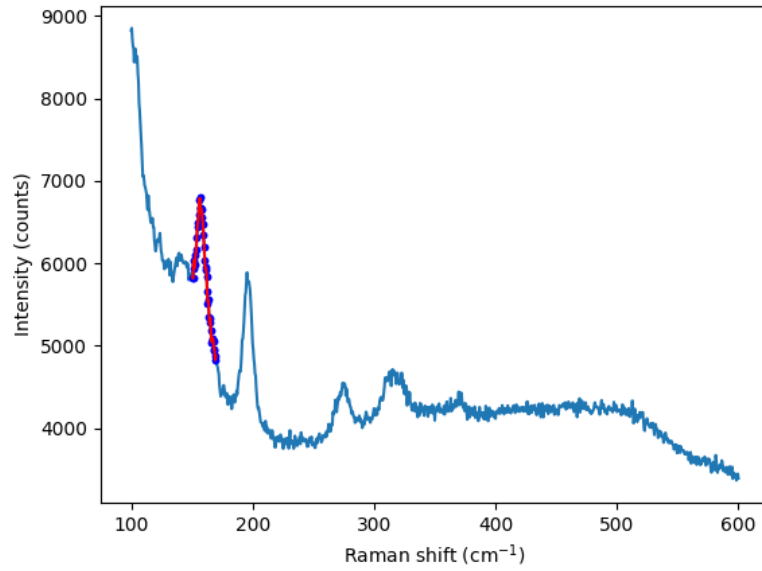


Figure 3.5: The Observed Raman peak at  $157.5 \text{ cm}^{-1}$  resulting from  $A_{1g}$  vibrational mode of the grown  $\text{Bi}_2\text{O}_2\text{Se}$

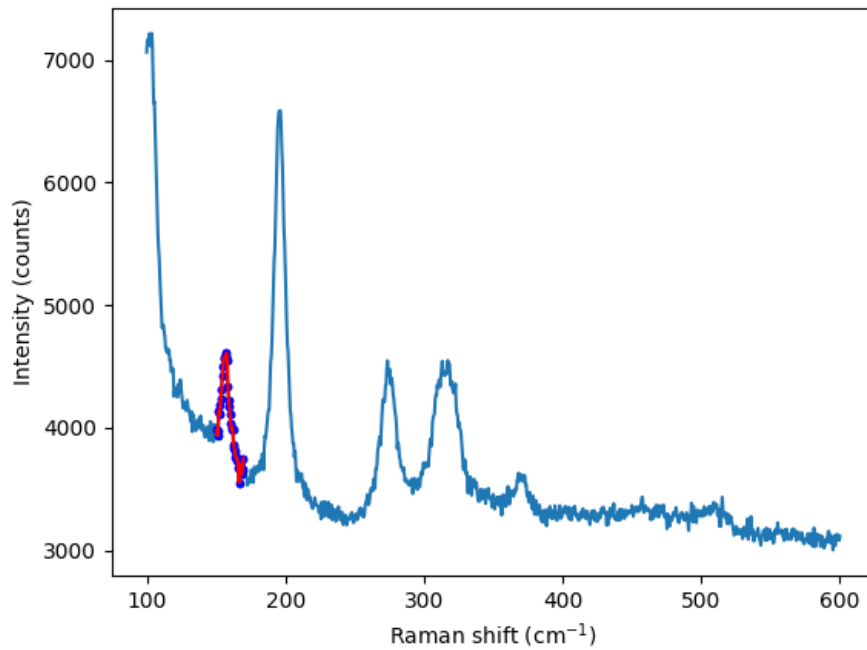


Figure 3.6: The Observed Raman Spectra of the grown  $\text{Bi}_2\text{O}_2\text{Se}$

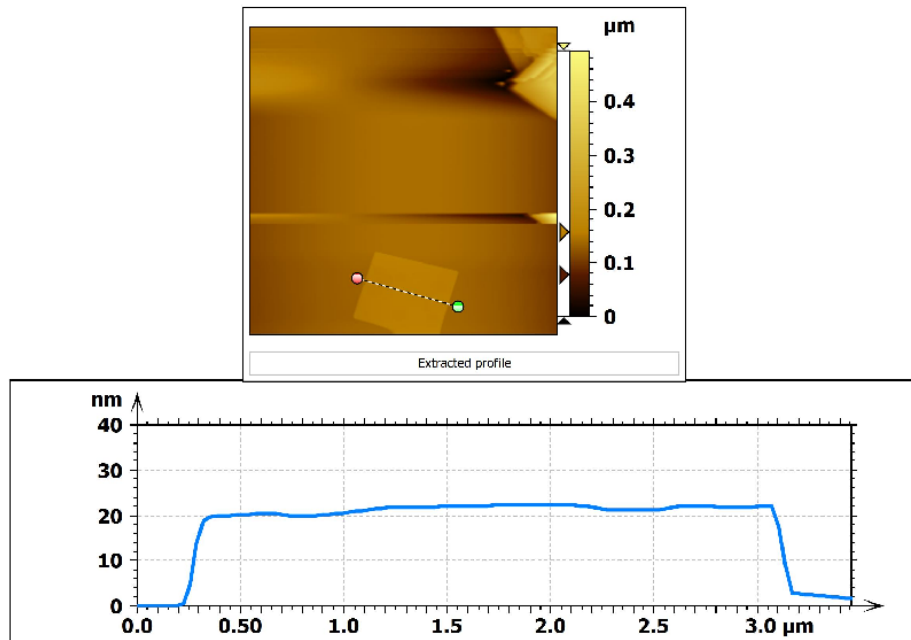


Figure 3.7: a) AFM images of crystals of Bi<sub>2</sub>O<sub>2</sub>Se grown on mica and the following thickness profile of the same(few layers)

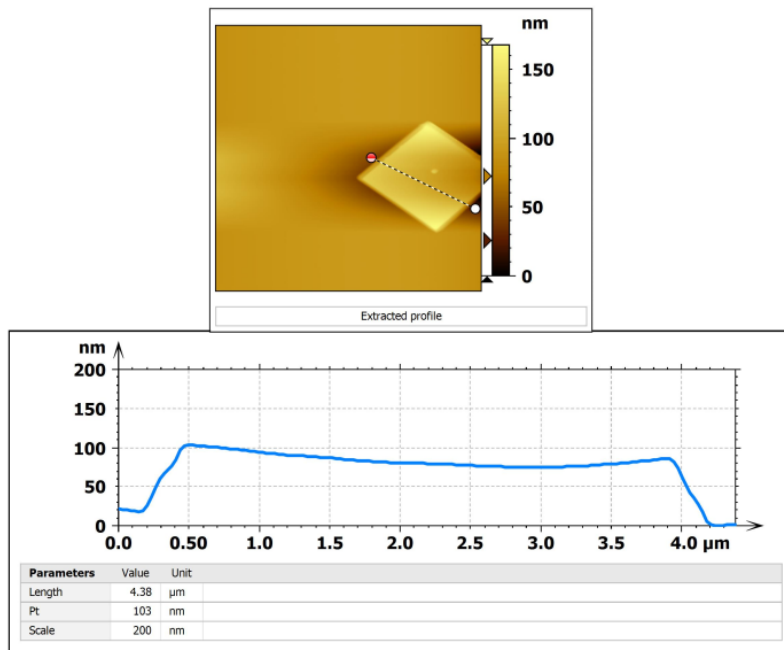


Figure 3.8: a) AFM images of crystals of Bi<sub>2</sub>O<sub>2</sub>Se grown on mica and the following thickness profile of the same(nanoplates)

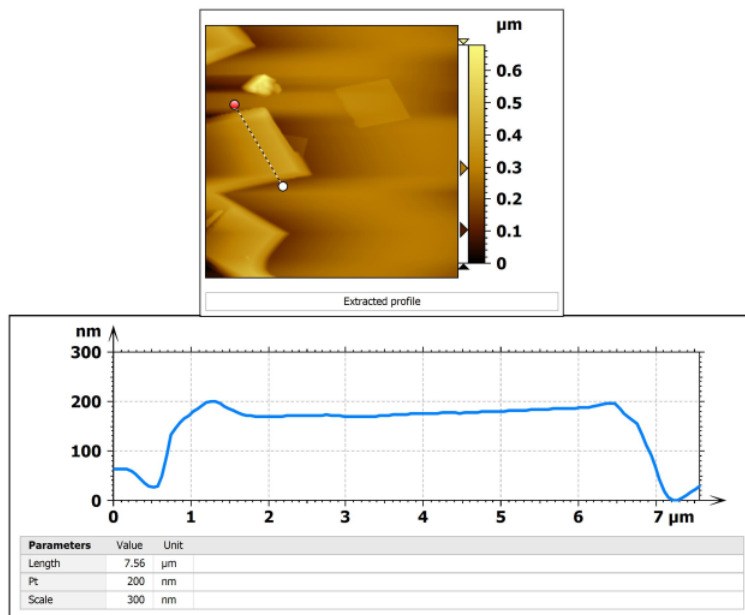


Figure 3.9: a) AFM images of crystals of  $\text{Bi}_2\text{O}_2\text{Se}$  grown on mica and the following thickness profile of the same(thick plates)

different substrates like muscovite mica, Au-coated Si, glass, and even directly onto the  $\text{SiO}_2$  coated Si. Here, we present some initial positive results.

## 3.2 The Initial "positive" Results of an Unsuccessful Project

Since, the Raman spectrum of the  $\text{Bi}_2\text{O}_2\text{Se}$  nanosheet shows a typical characteristic peak located around  $159\text{ cm}^{-1}$  resulting from  $A_{1g}$  vibrational mode, and the nanosheets grown on both f-mica and Si showed a prominent peak around  $160\text{ cm}^{-1}$  [19], thus we explored the CVD growth with various parameters and conditions.

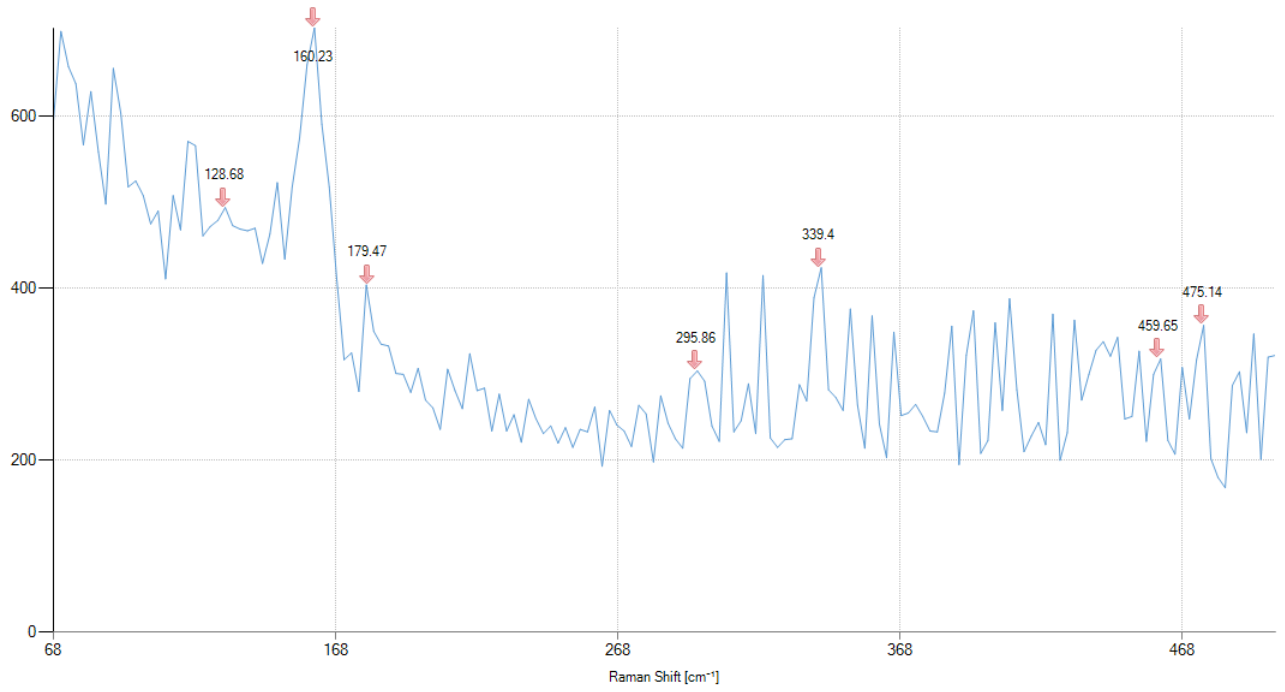


Figure 3.10: The Raman Spectra of thick plates grown on Si

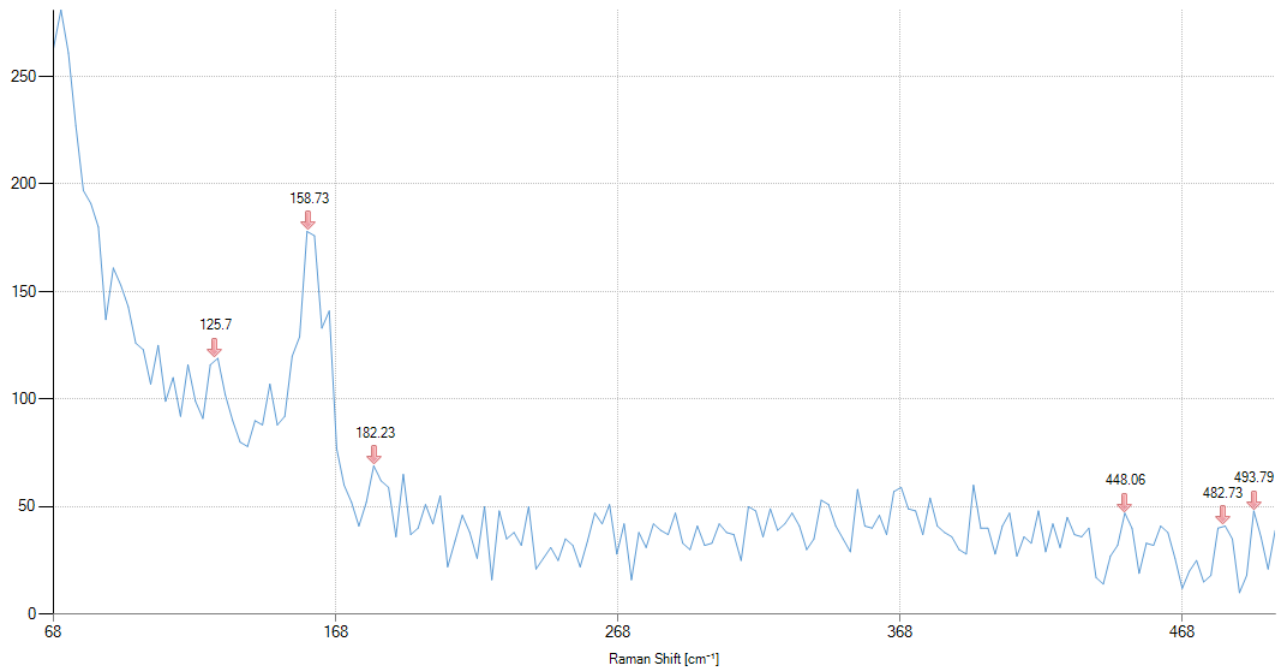


Figure 3.11: The Raman Spectra of thin plates grown on f mica in the same trial as above

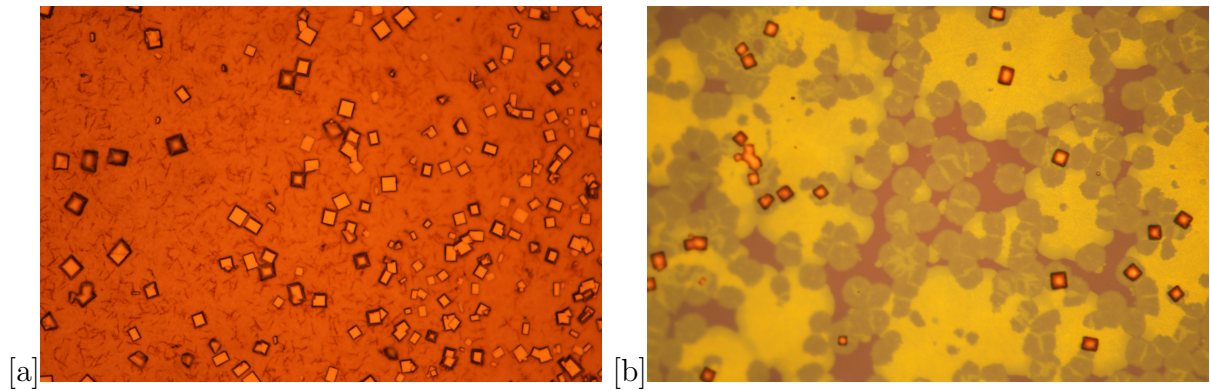


Figure 3.12: Optical Images of the CVD Growth of  $\text{Bi}_2\text{O}_2\text{Se}$  crystals on a) Gold coated Si substrate at 100x, b) Only on Si substrate 100x

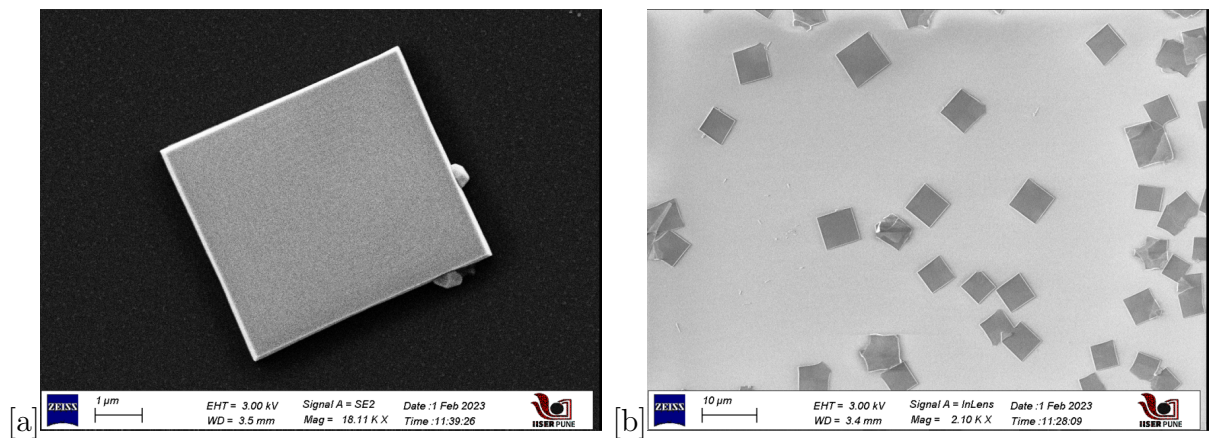


Figure 3.13: FSEM images of the CVD Growth of thin crystals of  $\text{Bi}_2\text{O}_2\text{Se}$  on Si substrate

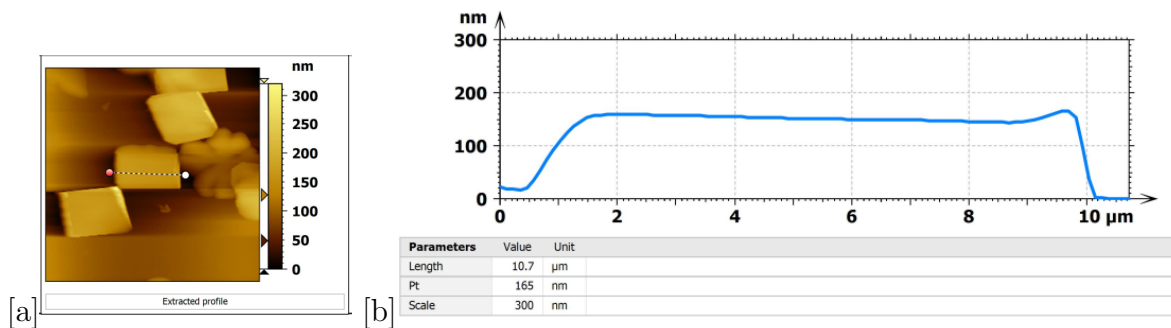


Figure 3.14: a) AFM images of crystals of  $\text{Bi}_2\text{O}_2\text{Se}$  grown on Si b) The thickness profile of a  $\text{Bi}_2\text{O}_2\text{Se}$  crystal



# Chapter 4

## Automated Maskless

## Photolithography Setup (AMPS)

### 4.1 The Existing Photolithography Setup

We have already discussed the working principle of UV Lithography, which is an advanced version of "visible range" (current setup) photolithography, but there are some caveats we should keep in mind regarding the relation between the intensity profile (Intensity vs. Frequency curve) of the light source and absorbance spectra of a photoresist. Since we use incandescent light as the light source, we must use filters to cut the wavelengths around the spectral absorbance peak to prevent the whole substrate from overexposing. (for example, the maxima of spectral absorbance of one of the commercially available negative photoresists lies around 310nm-430nm. [Sigma Aldrich](#)) Moreover, we use another filter to lower the overall intensity while we look for the coordinates of the other. As we have to do each step manually, the system is very prone to nonuniform exposure, ultimately reducing the contact quality and, thus, our device. But we need a lot of devices even to study a known phenomenon in known material to make any conclusion concrete, and that makes the usual photolithography

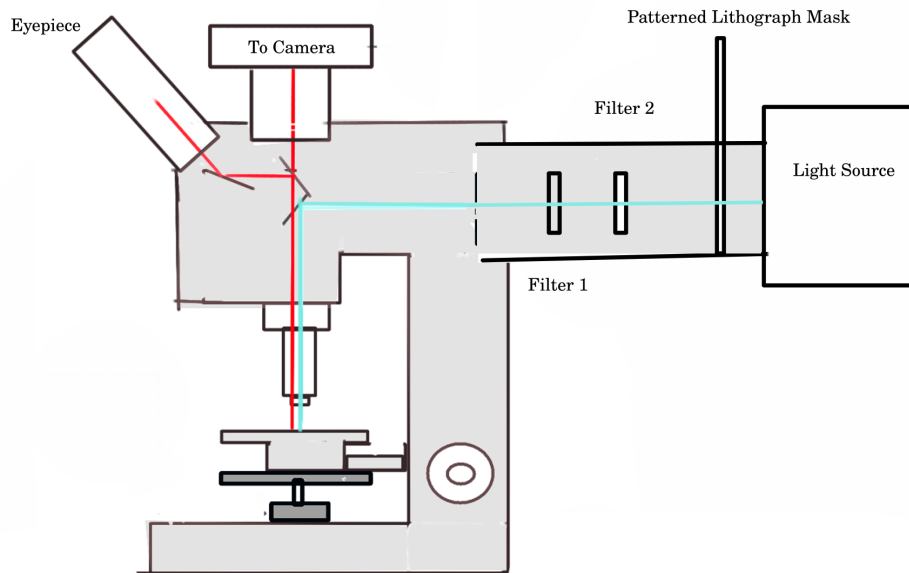


Figure 4.1: Schematic of the current photolithography setup

a slowing step in the research, which has already been solved but not for most of us. Another issue is the need for an already patterned photomask; thus, it limits us to only a handful of device configurations.

As Bismuth oxyselenide is not a VdW material, the CVD-grown and transferred material layer varies significantly in thickness and size. On top of that, using a fixed-size patterned mask limits us to only limited nanoplates or even monolayers, making the usual photolithography even more tedious and less efficient. Hence, we propose modifying the current setup to make the photolithography more automated and precise.

## 4.2 The Proposed Modifications

We can see the changes in schematics, it is as follows:

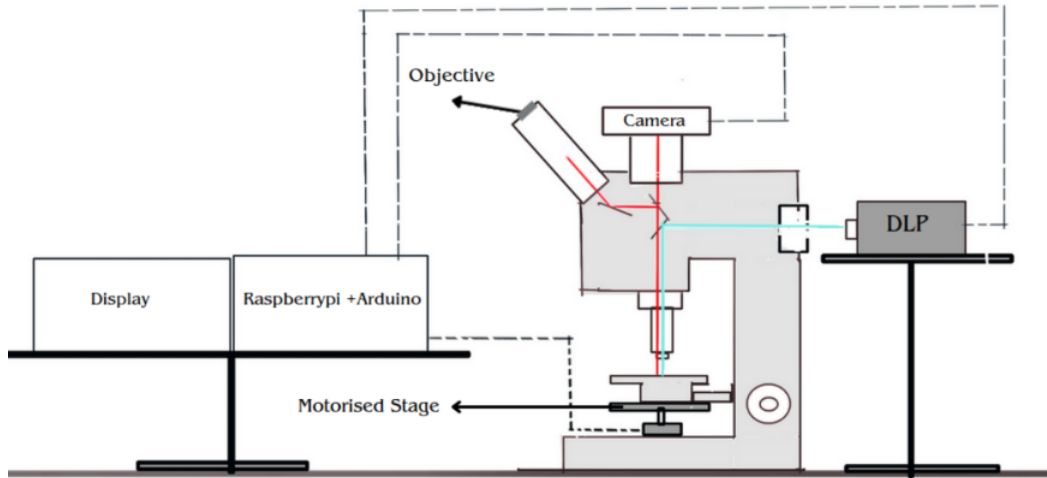


Figure 4.2: The Schematic of the Automated Maskless Photolithography Setup

- **Replacing the lamp with a DLP Projector:** We are using DLPDLCR230NPEVM (DLP® LightCrafter™ Display 230NP evaluation module), which is compatible with Raspberry Pi, by adding this alone, we can make our usual photolithography maskless by projecting any pattern we want to design. Moreover, the DMDs are powered by RGB LEDS (OSRAM red, green, and blue LED)(TI), giving us more precise control over even the intensity of the light, along with the freedom of photomasks
- **Making the stage motorized:** We modified the manual stage by attaching the stepper motors with belt pulleys, which can be precisely controlled in steps using Arduino UNO.
- **Using Camera instead of the objective:** The modern-day camera is a powerful tool that we will be using to get the coordinates in the nanometer scales from just the pixels.

## 4.3 Workflow of AMPS (Automated Maskless Photolithography System)

### 1. Initialization

- *State:* The system starts in the initial state with the camera focused at a reference point, typically a corner of the substrate.
- *Process:* The program is initiated. It captures images of the substrate by moving the camera in precise steps and stitches them together using OpenCV-Python's stitching algorithm.

### 2. Image Acquisition

- *State:* The system now has a complete image of the substrate.
- *Process:* Using machine learning object detection algorithms, the system identifies desired material structures across the substrate. The system can be trained to detect the number of layers of 2D materials through analysis and comparison with the image data.

### 3. Object Detection

- *State:* The program has the coordinates of each detected material flake.
- *Process:*
  - The system offers options to choose from a library of photomask designs or allows users to upload custom patterns.
  - Patterns are overlaid on each flake, and users have the flexibility to make adjustments.
  - Python's image edge detection tools are used to remove the background.

### 4. Programmed Photolithography

- *State:* The system now has an image with patterns overlaid on material flakes and their respective coordinates.
- *Process:*
  - The program translates coordinates into motor steps, considering the selected magnification, to establish the actual (x, y) coordinates with the initial reference point as the origin.
  - The stage is moved to focus on the coordinates, and simultaneously, a parallel code communicates with the DLP (Digital Light Processing) system to expose the relevant designed patterns on the corresponding coordinates.
  - It is essential to have optimized exposure times in advance.

## 5. Automation Completion

- *State:* The photolithography process continues till every assigned coordinate gets evenly exposed.

### 4.3.1 Workflow through Images

## 4.4 Instrumentation

### 4.4.1 The Electronics in detail

- **The Stepper Motor:** Stepper motors are electromechanical devices that operate by converting electrical pulses into precise mechanical motion. These motors work on the principle of digital control, meaning they move in discrete, fixed steps, making them ideal for applications requiring accurate positioning or control.

A stepper motor consists of a rotor and a stator, and the key to its operation lies in the arrangement of magnetic poles and windings within these components. By energizing

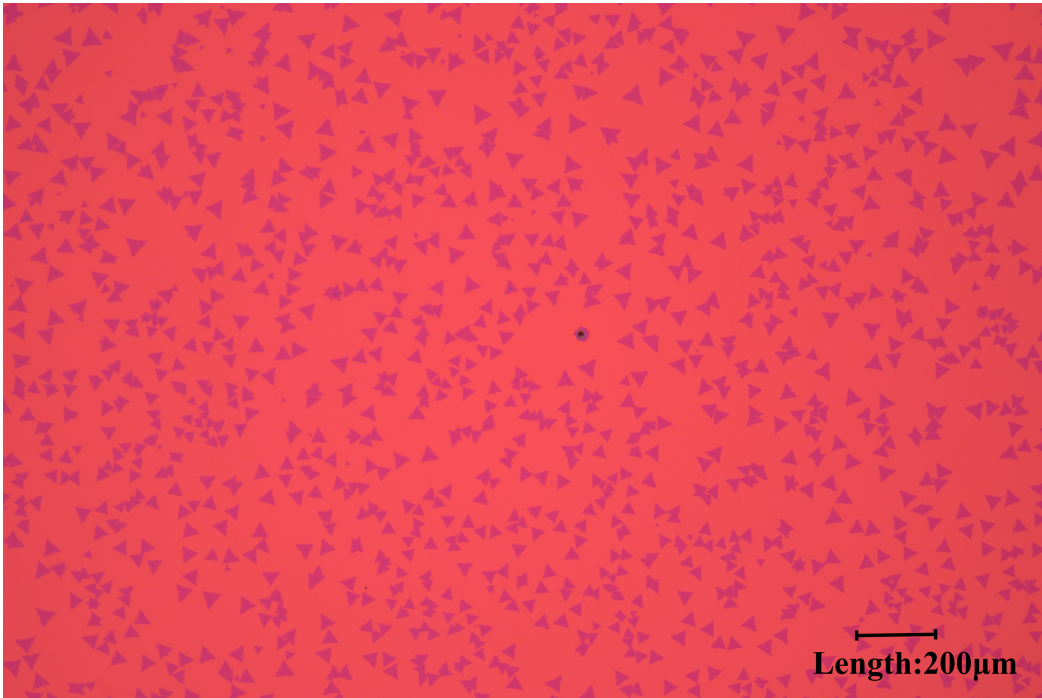


Figure 4.3: a) Image Acquisition

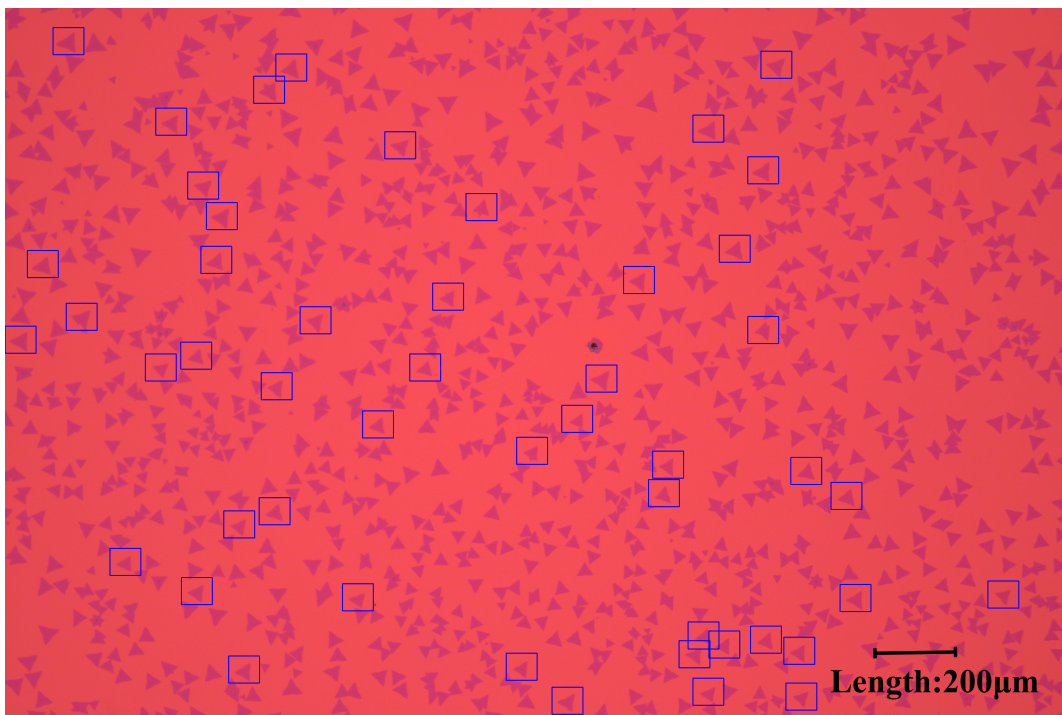


Figure 4.4: b) Object Detection

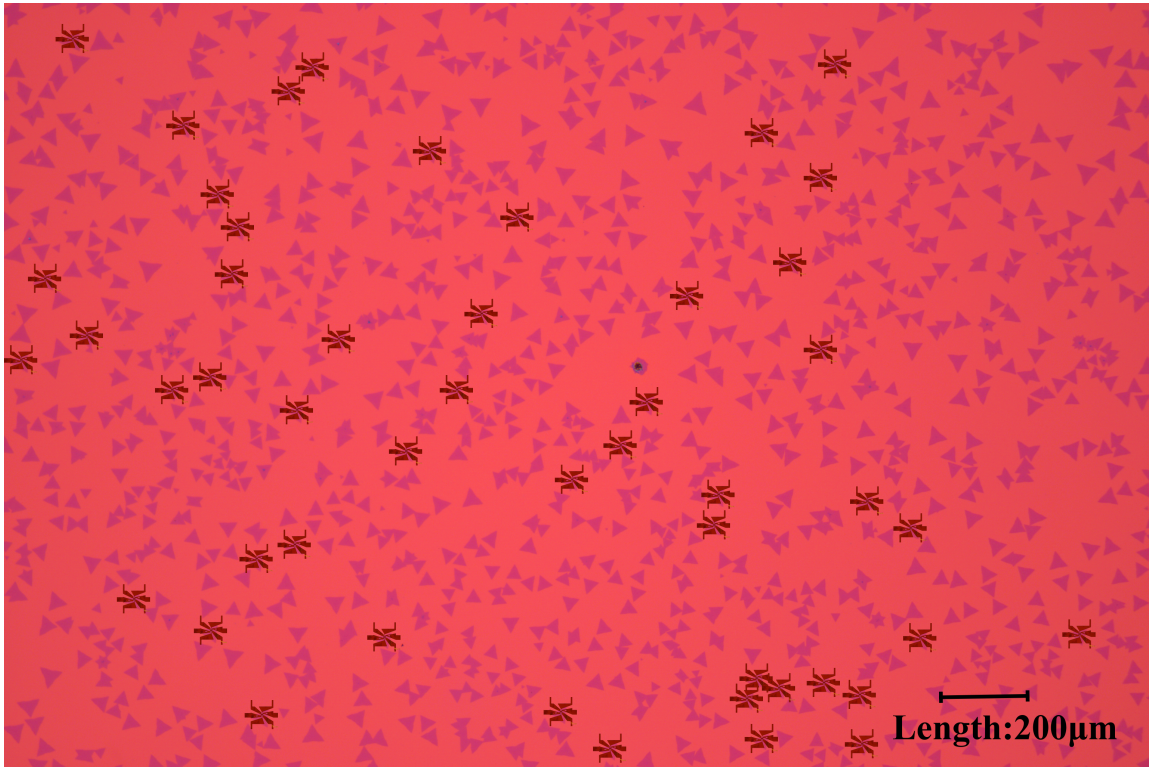


Figure 4.5: c) Programmed Photolithography

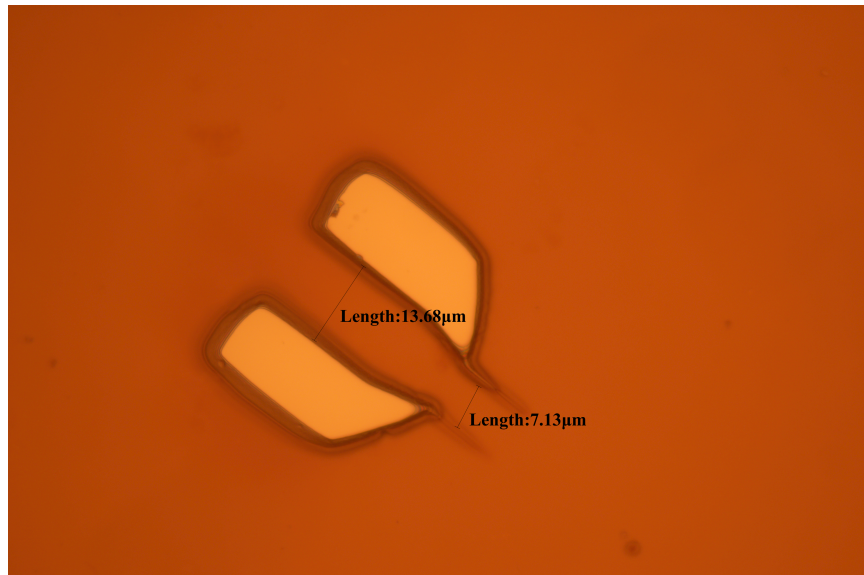


Figure 4.6: c) The initial results of the DLP Photolithography

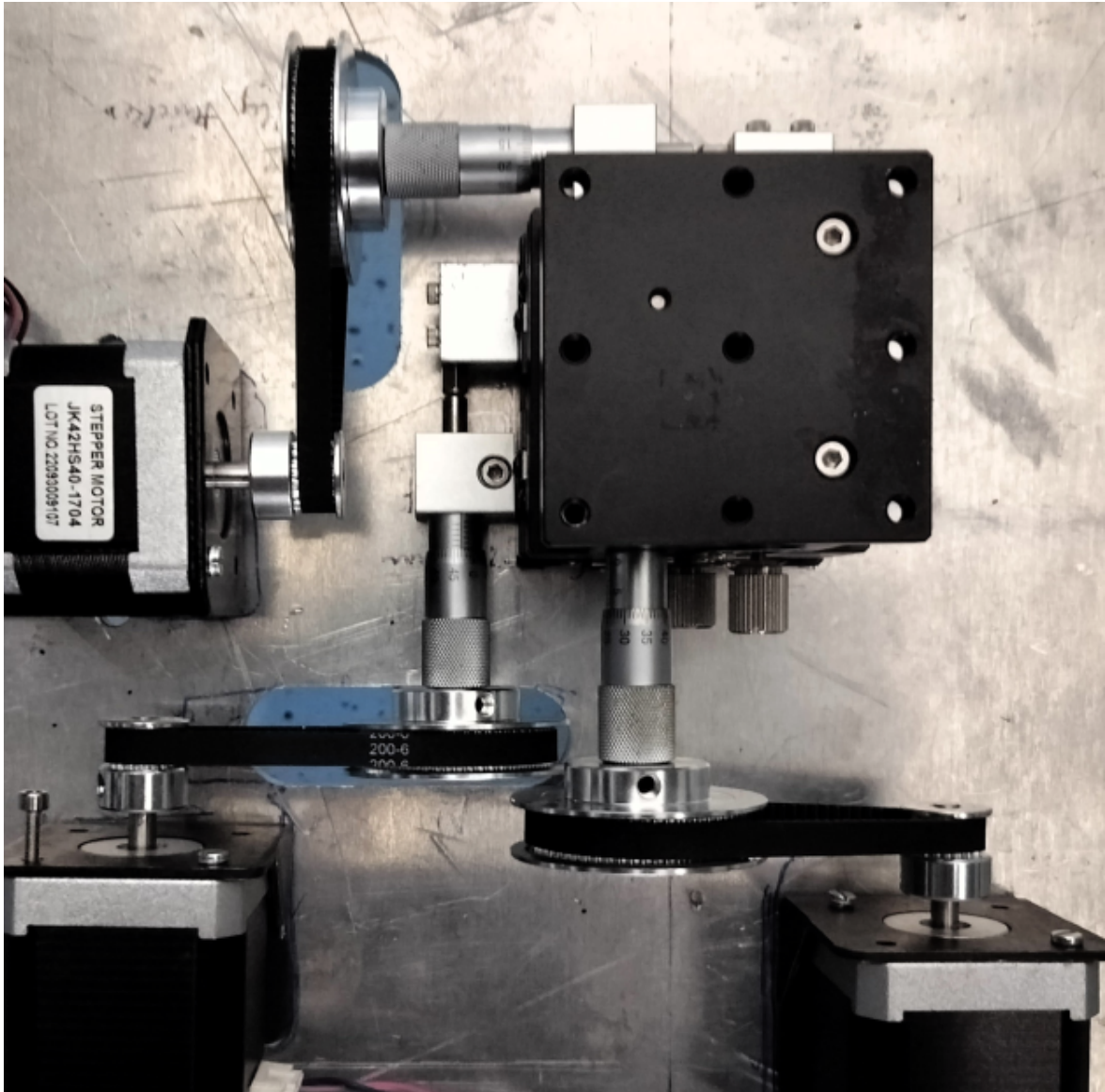


Figure 4.7: The motorized stage



specific stator windings in a controlled sequence, a magnetic field is generated, which interacts with the rotor's permanent magnets or teeth. This interaction causes the rotor to rotate by a fixed angle, known as a step. Stepper motors can have varying step sizes, typically expressed in degrees (e.g.,  $1.8^\circ$  or  $0.9^\circ$  per step) or steps per revolution (e.g., 200 or 400 steps per revolution) [20]. We are using NEMA17 motors.

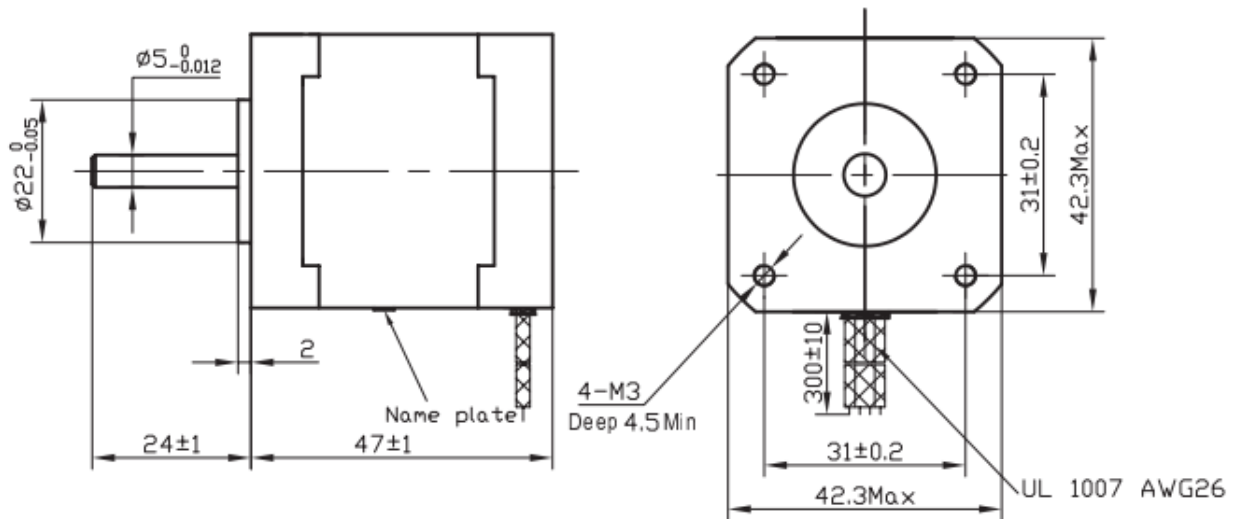


Figure 4.8: The schematic model of NEMA 17 motor

- **The A4988 driver: VDD:** This serves as the power input for the module, providing

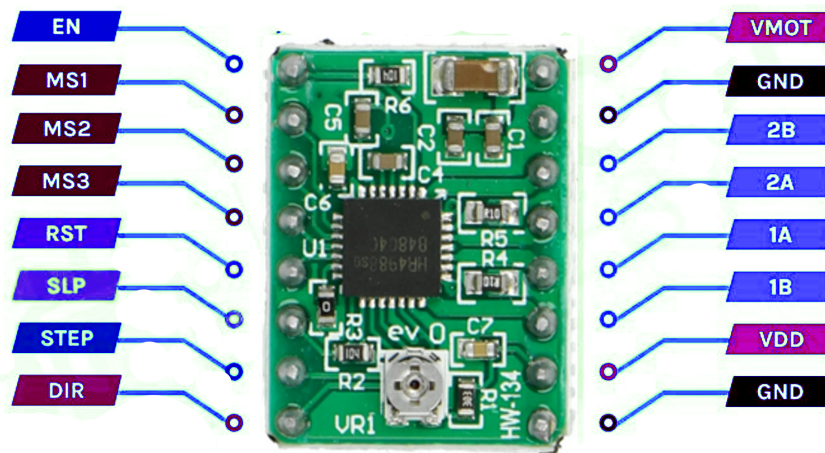


Figure 4.9: The schematic A4988 driver

the necessary voltage for its internal logic circuit. The voltage can vary within a range of 3.3V to 5.5V, associated with pin 10 on the module.

**GND:** The ground connection pin of the module links with the ground pin of the Arduino. Notably, the A4988 module contains two ground pins, which are numbered 9 and 16.

**VMOT:** The Motor Supply pin is responsible for delivering power to the motor. The allowable voltage range for this pin extends from 8V to 35V. According to the datasheet, it's important to place a suitable decoupling capacitor close to the board to ensure proper motor driver operation.

**MS1, MS2, MS3:** These pins select the microstepping resolution. The A4988 driver offers three inputs for choosing from five different step resolutions. By configuring these pins with the correct logic levels, you can set the motor to the desired step resolution.

**STEP:** This input governs the micro steps taken by the motor. Each HIGH pulse applied to this pin moves the motor in accordance with the number of micro steps dictated by the settings of the microstep selection pins. A higher pulse frequency results in a faster motor rotation.

**DIR:** This input determines the direction of motor rotation. Setting it to HIGH causes the motor to rotate clockwise, while a LOW signal makes it rotate counterclockwise.

**EN:** This input pin is active low. Pulling it LOW enables the A4988 driver. By default, this pin is already pulled low, meaning the driver is always enabled unless you manually remove it high. This feature is handy for implementing emergency stop or shutdown systems.

**SLP:** This is another active low-input pin. Setting it to LOW puts the driver into sleep mode, significantly reducing power consumption. This feature can conserve power when the motor is not in operation.

**RST:** Also an active low input, this pin serves two purposes. When pulled LOW, it causes the driver to ignore all STEP inputs. It also resets the driver by returning the

internal translator to a predefined "home" state. This "home" state represents the motor's initial position, which can vary depending on the chosen microstep resolution.

**1B, 1A, 2A, 2B:** These pins are the output channels of the A4988 motor driver, and they are accessible via pins on the module. You can connect small to medium-sized NEMA 17 motors to each output pin. Each output pin can deliver up to 2A of current to the motor. However, the actual amount of current supplied to the motor is contingent on factors like the power supply, cooling system, and current limiting settings within the system.

- **The Circuit Diagram:**

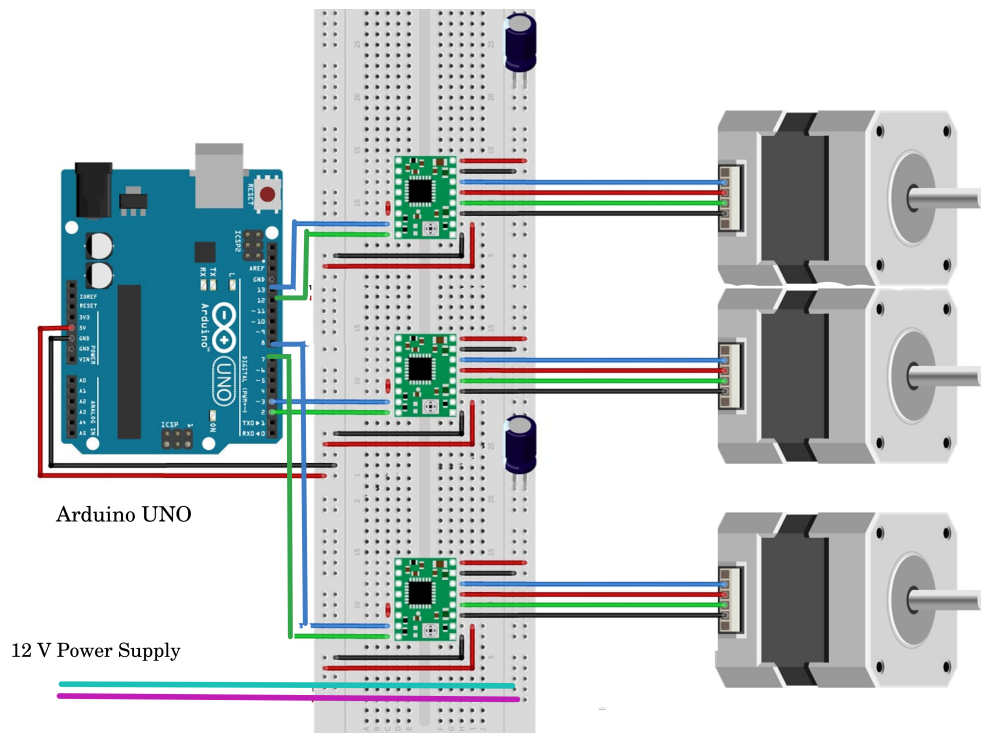


Figure 4.10: The circuit diagram for Stepper Motors

## 4.4.2 The Optics in detail

- The DLP Projector: Digital Light Processing (DLP) technology relies on a micro-electromechanical system (MEMS) device known as the Digital Micromirror Device™ (DMD™). Texas Instruments introduced the DMD in 1987. It's a semiconductor-based array of rapid, reflective digital light switches that accurately control a light source using binary pulse width modulation. Combined with image processing, memory, a light source, and optics, it forms a DLP system capable of projecting large, bright, seamless, and high-contrast color images [5]. The following schematic shows the overall working of DLP.

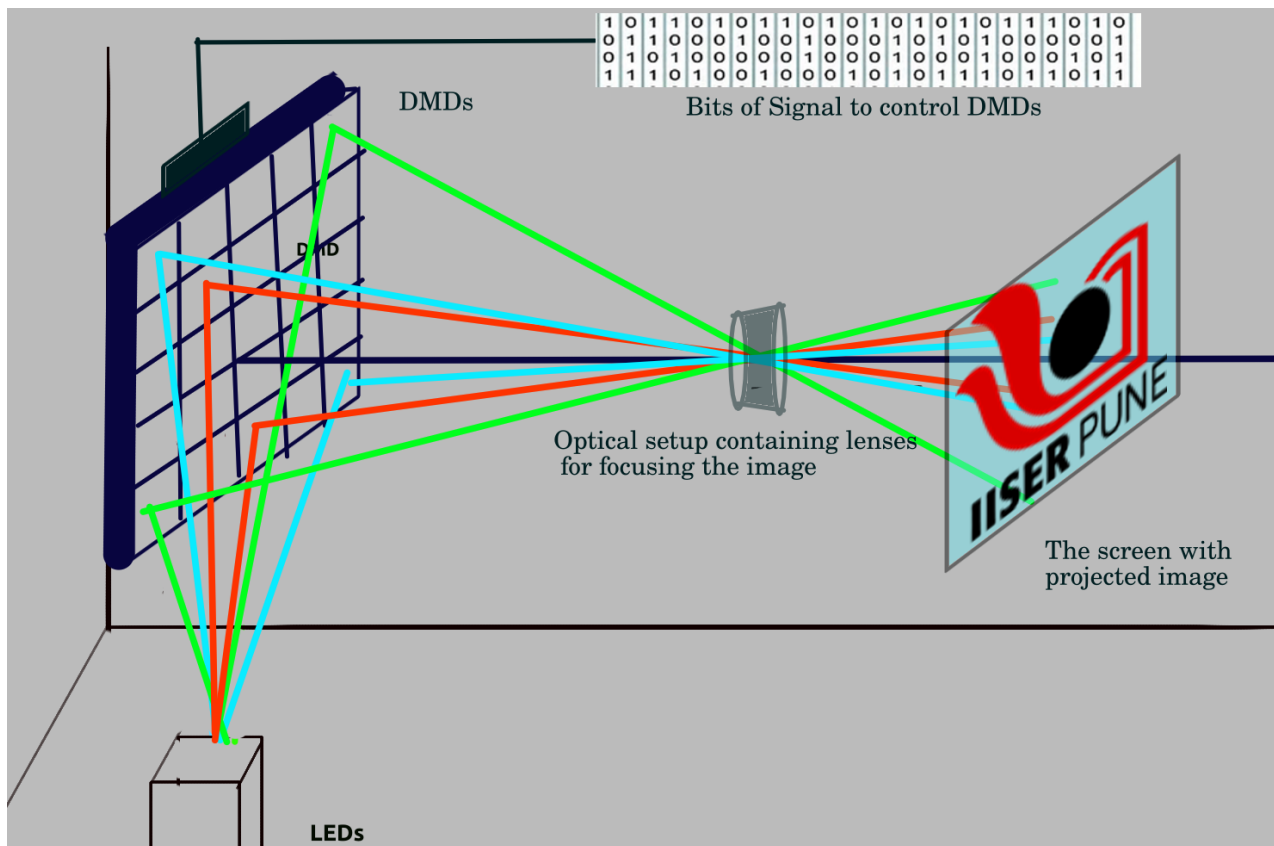


Figure 4.11: The schematic of Digital Light Processing

DLP-based projection displays are particularly well-suited for applications that require

high brightness and resolution for several reasons:

- 1. Reflective and High Fill Factor:** The digital light switch is reflective and has a high fill factor, resulting in high optical efficiency at the pixel level and minimal pixelation effects in the projected image.
- 2. Growing Efficiency with Resolution:** As the resolution and size of the DMD increase, the overall system's optical efficiency grows, thanks to higher lamp-coupling efficiency.
- 3. Compatibility with Conventional Voltage Levels:** The DMD operates with conventional CMOS voltage levels (around -5 volts), making it easy to employ integrated row and column drivers, thus minimizing complexity and cost when scaling to higher resolutions.

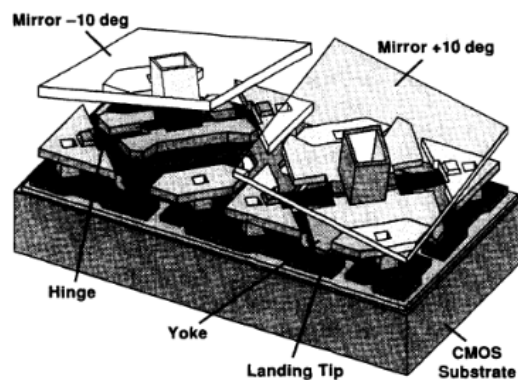


Figure 4.12: The two DMD pixels [5]

- 4. Effective Cooling:** As the DMD is a reflective technology, it can be efficiently cooled through the chip substrate. This feature enables the use of high-power projection lamps without the risk of thermal degradation of the DMD.
  - 5. Digital All the Way:** DLP-based systems are fully digital, accepting digital video input and delivering digital light output. This ensures accurate reproduction of the original video source material, resulting in stable and high-quality images over time.
- **The Microscope:** Optical microscopes utilize light, or photons, as their illumination

source. They operate based on the principle that by illuminating an object with light and observing the contour of the transmitted or reflected light, the object's shape becomes visible. An optical microscope comprises essential optical components, including a light source and one or more optical lenses to focus light onto an object to create its image. These optical microscopes come in two primary categories: simple optical microscopes, which have a single lens, and compound optical microscopes, equipped with multiple lenses. Compound optical microscopes typically consist of an objective lens, an ocular lens, and a condenser lens, among others.

The microscope's ability to resolve fine details is determined by various factors, including the wavelength ( $\lambda$ ) of the illumination light, the light collection angle ( $\theta$ ) governed by the objective lens, and the refractive index ( $n$ ) of the medium located between the lens and the sample. The resolution of optical microscopes can be described using different parameters, such as the Rayleigh diffraction limit and Abbe's diffraction limit. These components and principles collectively enable optical microscopes to unveil intricate details of microscopic specimens [21].

### 4.4.3 The Mechanics



Figure 4.13: Aluminium Timing Pulleys a) 6mm Belt Width 60 teeth b)6mm Belt Width 20 Teeth

We have observed that it takes two complete rotations(120 teeth covered) of the larger

timing pulley(44 mm) to move the stage by 1 mm, for all xyz directions, which corresponds to 0.008mm of step movement with the per teeth movement of the timing pulley.





# Chapter 5

## Conclusion and Future Prospects

We have successfully optimized the CVD growth of Bismuth Oxyselenide on f-mica with varying sizes and thicknesses, and further characterization has been done. Moreover, we found some limitations in the existing photolithography setup, so we modified the setup. The next goal is to replace the current blue LED( $\lambda = 455nm$ ) of DLP with an ultraviolet LED( $\lambda \leq 300nm$ ) since most of the photoresist are more reactive with UV light, and with smaller wavelength, we can go to a finer resolution in the architecture of nanodevices.

### 5.1 Two-Dimensional $\text{Bi}_2\text{O}_2\text{Se}/\text{MoS}_2$ Heterostructures

Moreover, we plan to transfer the grown Bismuth Oxyselenide nanoplates grown on mica onto Si/SiO<sub>2</sub> substrate, and make the devices using AMPS, and study optoelectronic properties. We also have monolayers of MoS<sub>2</sub> grown by Dr. Vrinda Narayanan, a former labmate. Thus, we plan to make 2D MoS<sub>2</sub>-Bi<sub>2</sub>O<sub>2</sub>Se heterostructures.

Interlayer charge transfer (CT) resulting from band alignment is crucial in various optoelectronic applications, including photoluminescence modulation and improved photoconduc-

tion. A systematic approach to observing CT is the layer-by-layer integration of atomically thin materials with differing band alignments. While the stacking of van der Waals (vdW) materials has been widely studied, the stacking of vdW materials with non-van der Waals (nvdW) materials remains underexplored.

Here, we plan to introduce the stacking of a non-vdW two-dimensional (2D) Bi<sub>2</sub>O<sub>2</sub>Se layer onto a vdW 2D MoS<sub>2</sub> monolayer and investigate the interlayer coupling and CT at this 2D interface.

Remarkably, it has already been seen that CT from the 2D Bi<sub>2</sub>O<sub>2</sub>Se layer to the MoS<sub>2</sub> monolayer results in the quenching of photoluminescence (PL) in the MoS<sub>2</sub> layer and an increase in photoconduction. Low-temperature PL studies indicate that strong interlayer coupling enhances the CT process [22].

And with the AMPS, we can complete the photolithography required in the process.

# Bibliography

- [1] J. Rühle. And there was light: Prospects for the creation of micro- and nanostructures through maskless photolithography. *ACS Nano*, 11(9):8537–8541, 2017. PMID: 28910077.
- [2] Lei Zheng, Urs Zywietz, Tobias Birr, Martin Duderstadt, Ludger Overmeyer, Bernhard Roth, and Carsten Reinhardt. Uv-led projection photolithography for high-resolution functional photonic components. *Microsystems & nanoengineering*, 7(1):64, 2021.
- [3] D Meng and AR Boccaccini. Nanostructured biocomposites for tissue engineering scaffolds. *Biomedical Composites*, pages 509–546, 2010.
- [4] Matteo Altissimo. E-beam lithography for micro-/nanofabrication. *Biomicrofluidics*, 4(2), 2010.
- [5] Larry J Hornbeck. Digital light processing for high-brightness high-resolution applications. In *Projection Displays III*, volume 3013, pages 27–40. SPIE, 1997.
- [6] Andre K Geim and Konstantin S Novoselov. The rise of graphene. *Nature materials*, 6(3):183–191, 2007.
- [7] Konstantin S Novoselov, Vladimir I Fal ko, Luigi Colombo, Pr R Gellert, Matthias Georg Schwab, and Kwanpyo Kim. A roadmap for graphene. *nature*, 490(7419):192–200, 2012.
- [8] Xidong Duan, Chen Wang, Anlian Pan, Ruqin Yu, and Xiangfeng Duan. Two-dimensional transition metal dichalcogenides as atomically thin semiconductors: opportunities and challenges. *Chemical Society Reviews*, 44(24):8859–8876, 2015.
- [9] Meng Gao, Hubert Jean-Ruel, Ryan R Cooney, Jonathan Stampe, Mark de Jong, Maher Harb, German Sciaini, Gustavo Moriena, and RJ Dwayne Miller. Full characterization of rf compressed femtosecond electron pulses using ponderomotive scattering. *Optics express*, 20(11):12048–12058, 2012.
- [10] Chao Xie, Chunhin Mak, Xiaoming Tao, and Feng Yan. Photodetectors based on two-dimensional layered materials beyond graphene. *Advanced Functional Materials*, 27(19):1603886, 2017.

- [11] Xuesong Li, Weiwei Cai, Jinho An, Seyoung Kim, Junghyo Nah, Dongxing Yang, Richard Piner, Aruna Velamakanni, Inhwa Jung, Emanuel Tutuc, et al. Large-area synthesis of high-quality and uniform graphene films on copper foils. *science*, 324(5932):1312–1314, 2009.
- [12] Xidong Duan, Chen Wang, Anlian Pan, Ruqin Yu, and Xiangfeng Duan. Two-dimensional transition metal dichalcogenides as atomically thin semiconductors: opportunities and challenges. *Chemical Society Reviews*, 44(24):8859–8876, 2015.
- [13] J.-T. Wang. Chapter 7 - chemical vapor deposition and its applications in inorganic synthesis. In Ruren Xu and Yan Xu, editors, *Modern Inorganic Synthetic Chemistry (Second Edition)*, pages 167–188. Elsevier, Amsterdam, second edition edition, 2017.
- [14] Bekir Sami Yilbas, Abdullah Al-Sharafi, and Haider Ali. Chapter 3 - surfaces for self-cleaning. In Bekir Sami Yilbas, Abdullah Al-Sharafi, and Haider Ali, editors, *Self-Cleaning of Surfaces and Water Droplet Mobility*, pages 45–98. Elsevier, 2019.
- [15] Mikhail V Pugachev, Aliaksandr I Duleba, Arslan A Galiullin, and Aleksandr Y Kuntsevich. Micromask lithography for cheap and fast 2d materials microstructures fabrication. *Micromachines*, 12(8):850, 2021.
- [16] Yuanxuan Fang and Yunfei He. Resolution technology of lithography machine. In *Journal of Physics: Conference Series*, volume 2221, page 012041. IOP Publishing, 2022.
- [17] Christophe Vieu, F Carcenac, A Pepin, Y Chen, M Mejias, A Lebib, L Manin-Ferlazzo, L Couraud, and H Launois. Electron beam lithography: resolution limits and applications. *Applied surface science*, 164(1-4):111–117, 2000.
- [18] Shaurya Prakash and Junghoon Yeom. Chapter 4 - advanced fabrication methods and techniques. In Shaurya Prakash and Junghoon Yeom, editors, *Nanofluidics and Microfluidics*, Micro and Nano Technologies, pages 87–170. William Andrew Publishing, 2014.
- [19] Ting Cheng, Congwei Tan, Shuqing Zhang, Teng Tu, Hailin Peng, and Zhirong Liu. Raman spectra and strain effects in bismuth oxychalcogenides. *The Journal of Physical Chemistry C*, 122(34):19970–19980, 2018.
- [20] Ivan Virgala, Michal Kelemen, Alexander Gmitterko, and Tomas Liptak. Control of stepper motor by microcontroller. *Journal of Automation and Control*, 3(3):131–134, 2015.
- [21] Naomichi Yamamoto. Chapter 6 - analytical methods. In Naomichi Yamamoto, editor, *Fundamentals of Bioaerosols Science*, pages 295–358. Elsevier, 2023.

- [22] Md Tarik Hossain, Larionette PL Mawlong, Tadasha Jena, Abhilasha Bora, Upasana Nath, Manabendra Sarma, and PK Giri. Interlayer charge-transfer-induced photoluminescence quenching and enhanced photoconduction in two-dimensional  $\text{Bi}_2\text{O}_2\text{Se}/\text{MoS}_2$  type-II heterojunction. *ACS Applied Nano Materials*, 6(13):11023–11036, 2023.